Acceptances for space-based and ground-based fluorescence detectors, and inference of the neutrino-nucleon cross-section above 10^{19} eV

Sergio Palomares-Ruiz,* Andrei Irimia,† and Thomas J. Weiler‡

Department of Physics and Astronomy, Vanderbilt University, Nashville, Tennessee 37235-1807, USA

(Received 13 January 2006; published 14 April 2006)

Detection of ultrahigh energy neutrinos will be useful for unraveling the dynamics of the most violent sources in the cosmos and for revealing the neutrino cross-section at extreme energy. If there exists a Greisen-Zatsepin-Kuz'min (GZK) suppression of cosmic-ray events above $E_{\rm GZK} \sim 5 \times 10^{19}$ eV, as predicted by theory, then the only messengers of energies beyond $E_{\rm GZK}$ are neutrinos. Cosmic neutrino fluxes can initiate air-showers through interaction in the atmosphere, or in the Earth. Neutrino trajectories will be downgoing to nearly horizontal in the former case, and ''Earth-skimming'' in the latter case. Thus it is important to know the acceptances (event rate/flux) of proposed air-shower experiments for detecting both types of neutrino-initiated events. We calculate these acceptances for fluorescence detectors, both space-based as with the EUSO and OWL proposals, and ground-based, as with Auger, HiRes and Telescope Array. The neutrino cross-section $\sigma_{\nu N}^{\rm CC}$ is unknown at energies above 5.2×10^{13} eV. Although the popular QCD extrapolation of lower-energy physics offers the cross-section value of $0.54 \times 10^{-31}(E_\nu/10^{20}\ {\rm eV})^{0.36}\ {\rm cm}^2$, new physics could raise or lower this value. Therefore, we present the acceptances of horizontal (HAS) and upgoing (UAS) air-showers as a function of $\sigma_{\nu N}^{\rm CC}$ over the range 10^{-34} to $10^{-30}\ {\rm cm}^2$. The dependences of acceptances on neutrino energy, shower-threshold energy, shower length, and shower column density are also studied. We introduce a cloud layer, and study its effect on rates as viewed from space and from the ground. For UAS, we present acceptances for events over land (rock), and over the ocean (water). Acceptances over water are larger by about an order of magnitude, thus favoring space-based detectors. We revisit the idea of Kusenko and Weiler [Phys. Rev. Lett. **88**, 161101 (2002)] to infer $\sigma_{\nu N}^{\rm CC}$ at $E_\nu \gtrsim 10^{20}$ from the ratio of HAS-to-UAS events, and obtain favorable results. Included in our UAS calculations are realistic energy-losses for taus, and Earth-curvature effects. Most of our calculation is analytic, allowing insight into the various subprocesses that collectively turn an incident neutrino into an observable shower.

DOI: 10.1103/PhysRevD.73.083003 PACS numbers: 13.15.+g, 95.55.Vj, 95.85.Ry

I. INTRODUCTION AND PURPOSE

Detection of ultrahigh energy ($E_\nu > 10^{18}$ eV $\equiv$ EeV) neutrinos is important for several reasons. First of all, neutrino primaries are not deflected by magnetic fields and so should point back to their cosmic sources. This contrasts with cosmic rays, which are charged and follow bent trajectories. Secondly, well above the Greisen-Zatsepin-Kuzmin (GZK) energy of $E_{\rm GZK} \sim 5 \times 10^{19}$ eV [1,2], they may be the only propagating primaries. As such, they may be the only messengers revealing the ultimate energy reach of extreme cosmic accelerators, generally believed to be powered by black holes. Above $E_{\rm GZK}$, the GZK suppression [1–4] of cosmic rays results from the resonant process $N + \gamma_{\rm CMB} \to \Delta \to N + \pi$; $E_{\rm GZK}$ is the lab-frame energy corresponding to the kinematic threshold $\sqrt{s} = M_\Delta$ for excitation of the intermediate Δ resonance. A handful of cosmic-ray events have been detected with estimated energies exceeding 10^{20} eV. The record energy is the famous Fly's Eye event at 3×10^{20} eV [5]. The observable neutrino spectrum could extend to much higher energies. Thirdly, in contrast to cosmic rays and photons, neutrinos are little affected by the ambient matter surrounding the central engines of Nature's extreme accelerators. Accordingly, neutrinos may carry information about the central engine itself, inaccessible with other primaries. In principle, neutrinos may be emitted from close to the black hole horizon, subject only to energy loss due to gravitational redshifting. An analogy can be made to solar studies performed with photons versus neutrinos. The photons are emitted from the outer centimeter of the Sun's chromosphere, while the neutrinos are emitted from the central core where fusion powers the Sun. Fourthly, neutrinos carry a quantum number that cosmic rays and photons do not have—flavor. Neutrinos come in electron, muon, and tau flavors. One may think of this ''extra'' flavor degree of information as the neutrino's superb analog to polarization for the photon, or nucleon number A for the cosmic ray. Each of these attributes, flavor, polarization, and nucleon number, carries information about the nature and dynamics of the source, and about the environment and path length of the intergalactic journey. The flavor ratios of cosmic neutrinos are observable [6]. Several papers have recently analyzed the benefits that neutrino flavor identification offers for unraveling the dynamics of cosmic sources [7]. The fifth reason why ultrahigh energy neutrino primaries traveling over cosmic distances are interesting is that such travel allows studies of the fundamental proper-

*Electronic address: sergio.palomares-ruiz@vanderbilt.edu
†Electronic address: andrei.irimia@vanderbilt.edu
‡Electronic address: tom.weiler@vanderbilt.edu

ties of neutrinos themselves. For studying some properties of the neutrino, such as neutrino stability/lifetime [8], or pseudo-Dirac mass patterns [9], it is the cosmic distance that is essential; for other properties, it is the extreme energy that is essential. A clear example of the latter is any attempt to determine the neutrino cross-section at energies beyond the reach of our terrestrial accelerators.

In this paper we will examine the potential for cosmic-ray experiments designed to track ultrahigh energy air-showers by monitoring their fluorescence yield [10], to detect horizontal air-showers (HAS) and upgoing air-showers (UAS) induced by a cosmic neutrino flux. We will also study the ability of these experiments to infer the neutrino-nucleon cross-section $\sigma_{\nu N}$ at energies above 10^{19} eV, from the ratio of their UAS and HAS events. Such energies are orders of magnitude beyond the energies accessible to manmade terrestrial accelerators. From the point of view of QCD, such a cross-section measurement would be an interesting microscope into the world of small-x parton evolution. The neutrino cross-section above 10^{19} eV could agree with any of the various QCD-motivated extrapolations that have been published [11,12], or not. The cross-section could also be quite different than the extrapolations. For example, if a new threshold is crossed between terrestrial neutrino energies $\sim$100 GeV, and the extreme energies reached by cosmic rays, $\sim 10^{11}$ GeV, then the cross-section could much exceed the QCD extrapolations. On the other hand, saturation effects can significantly reduce the total cross-section at these very high energies [13]. The 9 orders of magnitude increase in lab energy reach corresponds to 4.5 orders of magnitude increase in center-of-momentum energy reach. Even the center-of-momentum energy at the e-p HERA collider is more than 3 orders of magnitude below the cosmic-ray reach. This remarkable energy reach of cosmic rays presents ample room for new physics beyond our standard model. Proposals for new physics thresholds in this energy region include low-scale unification with gravity, in which neutrino-nucleon scattering produces mini-black holes [14] and/or brane wraps [15], nonperturbative electroweak instanton effects [16], compositeness models [17], a low-energy unification scale in string inspired models [18], and Kaluza-Klein modes from compactified extra dimensions [19]. All of these models produce a much enhanced neutrino cross-section above the new threshold. Dispersion relations allow one to use low-energy elastic scattering to place constraints on the high-energy cross-section [20], but the constraints are quite weak.

For HAS and UAS, we provide analytical calculations of the event-rate to flux ratio as a function of $\sigma_{\nu N}$. This ratio is known as the ''instantaneous experimental acceptance,'' with units of area $\times$ solid angle. The time-averaged acceptance includes an experimental ''duty factor,'' the fraction of time that the experiment is functioning. We will not include the duty factor in our calculations of acceptances. We note that acceptances are also sometimes called ''apertures.''

Experimental acceptance offers a very meaningful figure of merit for statistical reach. One has merely to multiply an experiment's acceptance by Nature's flux to arrive at an event rate for the experiment. Multiplying again by the experiment's run time (including the duty factor), one obtains the total number of events. Acceptance times run time is termed the experimental ''exposure.''

The acceptances we calculate are scalable to large area experiments such as HiRes, Auger, and in the near future Telescope Array, which are anchored to the ground, and to superlarge area experiments such as EUSO and OWL, which are proposed to orbit the Earth from space. A horizontal shower, deeply initiated, is the classic signature for a neutrino primary. The weak nature of the neutrino cross-section means that horizontal events begin where the atmospheric target is most dense, low in the atmosphere. In contrast, the ultrahigh energy pp cross-section exceeds 100 mb, so the air-nucleon cross-section exceeds a barn. Even the vertical atmospheric column density provides hundreds of interaction lengths for a nucleon, and so the cosmic-ray interacts high in the atmosphere. The weak nature of the neutrino cross-section also means that the event rate for neutrino-induced HAS is proportional to the neutrino-nucleon cross-section.

For a neutrino-induced UAS, the dependence on neutrino cross-section is more complicated, and more interesting. The Earth itself is opaque for neutrinos with energies exceeding about a PeV of energy. However, ''Earth-skimming'' neutrinos, those with a short enough chord length through the Earth, will penetrate and exit, or penetrate and interact. In particular, there is much interest in the Earth-skimming process $\nu_\tau \rightarrow \tau$ in the shallow Earth, followed by τ decay in the atmosphere to produce an observable shower. In Ref. [21] it was shown that the rate for the Earth-skimming process $\nu_\tau \rightarrow \tau$ is *inversely* proportional to $\sigma_{\nu N}$. There it was emphasized that $\sigma_{\nu N}$ could be inferred from a measurement of the ratio of HAS to UAS rates.[1] Of course, an implicit assumption is that there is enough neutrino flux at extreme energies to generate HAS and UAS event samples.

The inverse dependence of UAS rate on $\sigma_{\nu N}$ is broken by the $\tau \rightarrow$ shower process in the atmosphere. As the cross-section decreases, the allowed chord length in the Earth increases, and the tau emerges with a larger angle from the Earth's tangent plane. This in turn provides a smaller path length in air in which the tau may decay and the resulting shower may evolve. This effect somewhat mitigates the inverse dependence of the UAS on $\sigma_{\nu N}$.

[1]The prospects of inferring the neutrino-nucleon cross-section in the energy range of 100 TeV–100 PeV at neutrino telescopes such as IceCube, were studied in Ref. [22]; prospects at higher energies were studied in Ref. [23] for the Auger observatory.

TABLE I. List of variables and their meaning. (Conversion between variables z and w is given by $w\cos\theta = z$).

L	Chord length of ν trajectory through Earth
$z_{\rm int}$	Vertical height (depth) of HAS (UAS) ν interaction
$z_{\rm dk}$	Altitude of upgoing ν_τ decay (no Earth curvature)
$z'_{\rm dk}$	Altitude of upgoing ν_τ decay including Earth curvature
z_U	Maximum visible-shower altitude (HAS $\neq$ UAS)
z_L	Minimum visible-shower altitude (HAS $\neq$ UAS)
z_B	Altitude where shower first attains threshold brightness (HAS $\neq$ UAS)
z_E	Altitude where shower extinguishes (HAS $\neq$ UAS)
$z^{\rm crit}_{\rm cloud}$	Critical altitude for suppression from cloud layer
z'_B(UAS)	Altitude where UAS attains threshold brightness, including Earth curvature
z'_E(UAS)	Altitude where UAS extinguishes, including Earth curvature
θ_z	Zenith angle of HAS event
θ_n	Nadir angle of UAS event (no Earth curvature)
$\theta_{\rm hor} = \frac{\pi}{2} - \theta_z$	Horizontal angle of UAS event
θ'_n	Nadir angle of UAS event including Earth-curvature
$\theta'_{\rm hor}$	Horizontal angle of UAS event including Earth curvature
$d_{\rm tot}$	Total column density along chord of Earth
d_ν	Column density of ν in the Earth
d_τ	Column density of τ in the Earth
$\cos\theta^*_{\rm S}$	Minimum shower angle, cloud dependent, for space observatory
$\cos\theta^*_{\rm G}$	Minimum shower angle, cloud dependent, for ground observatory
$\hat{z}$(HAS)	Maximum altitude from which initiated HAS can reach the ground
$\hat{z}$(UAS)	Minimum altitude from which initiated UAS can reach $z_{\rm thin}$
$\hat{z}'$(UAS)	$\hat{z}$(UAS) with Earth curvature included
$\hat{z}$(UAS $\otimes$ G)	$\hat{z}$(UAS) modified for cloud layer above
$\hat{z}$(HAS $\otimes$ S)	$\hat{z}$(HAS) modified for cloud layer below

Reference [21] provided an approximate calculation of the whole UAS process, and gave an approximate result for the dependence of the HAS/UAS ratio on $\sigma_{\nu N}$. In this work, we improve upon Ref. [21] in several ways. We include the energy dependences of the tau energy losses in the Earth, and of the tau lifetime in the atmosphere. For the energy losses, we distinguish between tau propagation in earth rock and propagation in ocean water. These calculations are carried out in Sec. II. On the issue of shower development, we incorporate the dependence of atmospheric density on altitude. We also impose requirements on the resulting shower such that a sufficiently long visible shower length is projected onto the Earth's tangent plane, thus meeting experimental requirements for visibility. This is done in Sec. III. In the case of the upgoing showers, the path length of the predecayed tau may be so long that the Earth's curvature enters into the altitude dependence. We include the non-negligible correction from curvature in Sec. III. We include the partial loss of visibility due to high cirrus or low cumulus cloud layers in Sec. IV. It is estimated that clouds will obscure the viewing area about 60%–70% of the time. For ground-based observation, it is mainly the low-lying cumulus clouds that limit visibility. For space-based observation, it is mainly the high cirrus clouds that limit visibility.[2] In Sec. V, we combine the corrections from clouds with that from the Earth's curvature.

Our results are illustrated in a series of plots of acceptances, for ground-based and space-based experiments, versus neutrino-nucleon cross-section, in Sec. VI. Situations with and without cloud layers are analyzed, as are events over solid earth and over the ocean. Incident neutrino energies, energy thresholds for experimental detection of the air-shower, and various shower-trigger parameters are varied. Earth-curvature effects are included in our UAS calculations. These reduce the event rate. Next comes the discussion in Sec. VII. It presents several small issues, and includes a comparison of our work with prior work. A final section recaps our conclusions. Some of the more tedious but necessary formulas are derived in an Appendix.

The reader who believes that a picture (or four) is worth a thousand words may wish to jump to Sec. VI. Such a reader especially may find it useful to reference Tables I and II, where the variables and parameters are defined.

Among our conclusions, we find that the HAS/UAS ratio is of order of unity for cross-section values very near to the

[2]In fact, low-lying cumulus clouds may aid in HAS identification for space-based observing. When the HAS hits the cloud layer, diffuse reflection of the forward Čerenkov cone can be seen as a one-time "Čerenkov flash." The time of the flash and the measured height of the cloud then provide the absolute (t, z) coordinates of the shower.

TABLE II. List of parameters, their meaning, and their chosen value(s); the bold-faced value is the chosen ''canonical'' value.

h	Scale height of the atmosphere	8 km
$z_{\rm ground}$	Ground altitude, kept as a symbol for later substitutions	0
$z_{\rm thin}$	Altitude beyond which air is too thin to fluoresce significantly	$3h$
β_{19}	Tau energy-attenuation constant at $E_\tau = 10^{19}$ eV	$1.0(0.55) \times 10^{-6}$ cm^2/g for rock (water)
α	Exponent of the energy-dependence of β_τ	0.2
$d_{\rm vert}$	Vertical atmospheric column density	1, 030 g/cm^2
$d_{\rm hor}$	Horizontal atmospheric column density	37 100 g/cm^2
$d_{\rm min}$	Minimum acceptable shower column density	300, **400** g/cm^2
$d_{\rm max}$	Maximum shower column density at extinction	**1200**, 1500 g/cm^2
$l_{\rm min}$	Minimum acceptable shower length projected on the Earth's surface	**10** km, 5 km
$R_{\rm FOV}$	Radius (or half-scale) of the experimental field of view	230 km
$z_{\rm w}$	Depth of ocean	3.5 km
$z_{\rm cloud}$	Altitude of cloud layer	**2**, 4, 8, 12 km
E_ν	Incident neutrino energy	$\mathbf{10^{20}}$, 10^{21} eV;
$E_{\rm th}^{\rm sh}$	Detector threshold energy	10^{19}, $\mathbf{5 \times 10^{19}}$
$E_{\rm th}^{\tau}$	Tau threshold energy	$\frac{3}{2}(3) \times E_{\rm th}^{\rm sh}$ for hadron (electron) mode
$\sigma_{\nu N}^{\rm CC}$	Neutrino (or WIMP) cross-section	10^{-30}, $\mathbf{10^{-31}}$, 10^{-32}, 10^{-33} cm^2

commonly extrapolated value of 0.5×10^{-31} cm^2 at $E_\nu \sim 10^{20}$ eV. This is fortunate, for it offers the best possibility that both HAS and UAS rates can be measured, and a true cross-section inferred. We display our HAS and UAS acceptance plots for a cross-section range from superweak 10^{-34} cm^2 to a microbarn, 10^{-30} cm^2. This range includes the QCD extrapolations of $\sigma_{\nu N}^{\rm CC}$, and the region of the HAS/UAS crossover. It also encompasses any effects of new neutrino physics, either increasing or decreasing $\sigma_{\nu N}^{\rm CC}$. The highest energy for which the neutrino cross-section has been measured is that at the HERA accelerator. The measurement is $\sigma_{\nu N}^{\rm CC} \sim 2 \times 10^{-34}$ cm^2 at $\sqrt{s} = 314$ GeV [24], the latter corresponding to an energy on fixed nucleon target of 5.2×10^{13} eV (52 TeV). It is hard to imagine that $\sigma_{\nu N}^{\rm CC}$ at 10^{20} eV would not have grown beyond the HERA value. Even so, the acceptances shown for superweak cross-sections may have some relevance to a possible WIMP flux [25]. Modeling of a WIMP event rate requires modifications in the shower development for HAS, and in the chain WIMP $\rightarrow$ UAS, that we do not pursue here.

II. AIR-SHOWER RATES

The variables and parameters needed to describe UAS and HAS are sufficiently numerous that we have collected many of them in Tables I and II for easy reference. In Table III we explain the different symbols used throughout this work. Many of the variables are best explained by the three schematic diagrams in Figs. 2–5.

TABLE III. List of symbols and their meaning.

HAS	Horizontal air-shower
UAS	Upgoing (''Earth-skimming'') air-shower
HAS $\otimes$ S	HAS seen from space-based observatory
UAS $\otimes$ S	UAS seen from space-based observatory
HAS $\otimes$ G	HAS seen from ground-based observatory
UAS $\otimes$ G	UAS seen from ground-based observatory

A. Upgoing air-showers (UAS)

Ultrahigh energy neutrinos are expected to arise from the decay of pions and subsequently muons produced in astrophysical sources [7]. For this decay chain, the flavor mix at the source is ν_e:ν_μ = 1:2. The maximal mixing between ν_μ and ν_τ inferred from terrestrial oscillation experiments then leads, after propagation for many oscillations lengths and to a very good approximation, to a flavor ratio at Earth of ν_e:ν_μ:ν_τ = 1:1:1, i.e., flavor democracy. Thus, a detector optimized for ν_e or ν_μ or ν_τ can expect a healthy signal from cosmic neutrinos.

It is useful to define the neutrino charged-current (CC) interaction mean-free path (MFP) as

$$\lambda_\nu = \frac{1}{\sigma_{\nu N}^{\rm CC} \bar{\rho}} = \frac{63 \text{ km}}{\rho_{2.65} \sigma_{31}} \tag{1}$$

where $\bar{\rho}$ is the mean number-density of the target matter, and $\rho_{2.65}$ is the mean density in units of the value for surface rock $\rho_{\rm sr} = 2.65$ g/cm^3. Density is usually expressed in units of g/cm^3, with the multiplicative factor of $N_{\rm A} = 6.022 \times 10^{23}$ g^{-1} implicitly understood. The mean density of ocean water is 1.0 g/cm^3. The cross-section σ_{31} is the CC cross-section in units of 10^{-31} cm^2. The commonly used high-energy neutrino-nucleon CC cross-section extrapolated from QCD [11] is $0.54 \times 10^{-31} (E_\nu/10^{20} \text{ eV})^{0.363}$ cm^2.

We will ignore the NC contribution to the neutrino MFP for three reasons. First, the NC cross-section is expected to be small compared to the CC cross-section, as it is known to be at the lower energies of terrestrial accelerators. Secondly, the NC interaction does not absorb the neutrino, but rather lowers the energy of the propagating neutrino by

a small amount; in the SM, the energy loss is only $\langle y \rangle \sim 20\%$. Thirdly, the increase in complexity of our calculation, when the NC MFP is included, seems unwarranted. We also ignore multiple CC interactions due to the "tau regeneration" decay chain $\nu_\tau \to \tau \to \nu_\tau$. Here, it is the long decay length of the tau that results from production at $E_\nu > 10^{17}$ eV that makes tau regeneration negligible.

In Fig. 1 we show an interesting relation between the neutrino cross-section, the neutrino's MFP in the Earth, and roughly speaking, the maximum horizontal angle for which the neutrino may transit the Earth.

In this figure, the Earth has been approximated according to the two-shell model. There is a central core with mean density 12 g/cm^3 out to a radius of 3486 km, and a mantle with mean density 4.0 g/cm^3 out to the Earth's radius of $R_\oplus = 6371$ km. The point of this figure is that, although the Earth is marginally transparent for neutrinos with the HERA cross-section of 2×10^{-34} cm^2, the Earth quickly becomes opaque at larger cross-section. For the cross-section values extrapolated to $\sim 10^{20}$ eV, horizontal angles are very small, and the trajectories are truly "Earth skimming" [cf. Eq. (7)].

The tau energy-attenuation length is $\lambda_\tau = (\beta_\tau \overline{\rho})^{-1}$, where $\beta_\tau(E)$ is the coefficient giving a scale to tau energy loss:

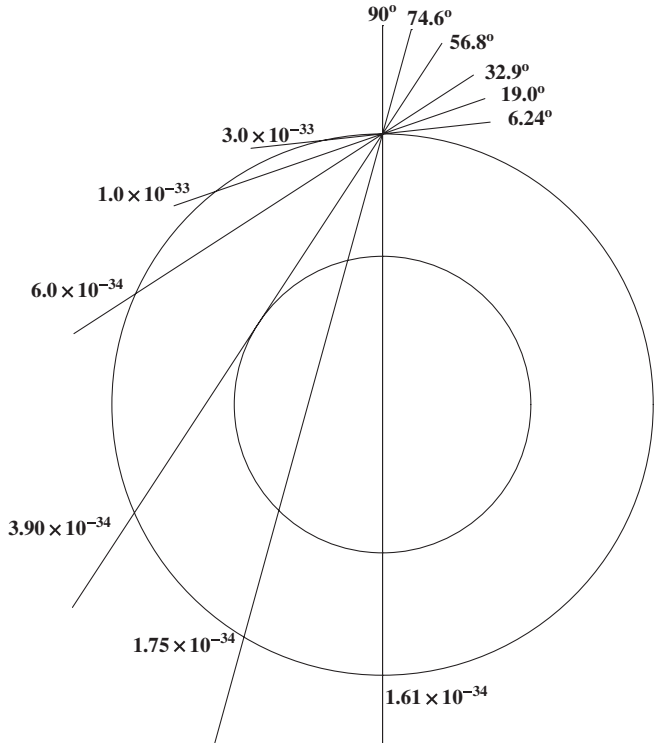

FIG. 1. Shown are neutrino trajectories for which the interaction MFP matches the chord length through the Earth. The various trajectories are parametrized by values of the neutrino cross-section. Also shown is the trajectory's angle with respect to horizontal.

$$dE_\tau/dx = -\beta_\tau(E)\rho E_\tau. \tag{2}$$

The coefficient $\beta_\tau(E)$ is weakly energy dependent. For the energies of interest, $E_\nu > 10^{18}$ eV, tau energy losses are dominated by photonuclear processes, with the electromagnetic mechanisms of ionization, bremsstrahlung and e^+-e^- pair production being negligible [26]. We find that the recent calculations of $\beta_\tau(E)$ [27–29] are well fitted in the energy region of interest by a simple power law [30]:[3]

$$\beta_\tau(E) = \beta_{19}\left(\frac{E_\tau}{10^{19}\ \text{eV}}\right)^\alpha, \qquad \alpha = 0.2, \tag{3}$$

with the constant prefactor $\beta_{19}^{\text{sr}} = 1.0 \times 10^{-6}$ cm^2/g for surface rock ($\langle A \rangle = 22, \langle Z \rangle = 11$), and $\beta_{19}^{\text{w}} = 0.55 \times 10^{-6}$ cm^2/g for water ($\langle A \rangle = 11.9, \langle Z \rangle = 6.6$); $\beta_\tau(E)$ scales as $\langle A \rangle$. The tau energy-attenuation length at $E_\tau = 10^{19}$ eV is $\lambda_\tau = 3.8$ km in surface rock, and 18 km in water. The tau decay MFP is $c\tau_\tau = 490(E_\tau/10^{19}\ \text{eV})$ km. For taus with energies at and above 10^{18} eV, the decay MFPs are much longer than the energy-attenuation length. In this paper, we safely neglect the small probability of decay within the Earth for those taus which would otherwise emerge from the Earth with energy above 10^{18} eV. We have checked that the results we present in this work are reduced by less than a few percent when the tau decay probability within the Earth is included.

The muon energy-attenuation length is 7 times smaller than that of the tau, and the electron energy-attenuation length is many times smaller again (the μ decay length is $\sim 10^8$ times longer than that of the tau). Because the energy-attenuation length for a tau is an order of magnitude longer than that of a muon, UAS events are dominantly initiated by the CC interaction of tau neutrinos.

The ratio of the tau energy-attenuation length to the neutrino MFP $\lambda_\tau/\lambda_\nu = N_A \sigma_{\nu N}^{\text{CC}}/\beta_\tau \sim (\sigma_{\nu N}^{\text{CC}}/10^{-31}\ \text{cm}^2) \times 0.06(0.11)$ for rock (water), is independent of ρ and only weakly dependent on tau energy. For $\sigma_{\nu N}^{\text{CC}} \lesssim 2 \times 10^{-30}$ cm^2, we expect most of the path length in Earth (rock or water) to be neutrino; for $\sigma_{\nu N}^{\text{CC}} \gtrsim 2 \times 10^{-30}$ cm^2, we expect most of the path length to be tau. In detail, this remark will also depend on the direction of the initial neutrino, i.e. on the total chord length, and on the threshold energy of the detector (the minimum recordable tau energy).

Consider a tau produced in the Earth along a chord on the trajectory of an incoming ν_τ. Label the chord length by L and the distance between the interaction and the Earth's surface by w_{int}, as shown in Fig. 2. In general, we will use the variable w to represent distance or location along the

[3]In a very recent paper [31], a logarithmic fit to $\beta_\tau(E)$ is presented. We find that our fit agrees quite well with that one in the region of our interest, $10^{18}\ \text{eV} \leq E_\nu \leq 10^{21}$ eV. For our purposes, the power-law fit is more useful in that it allows analytic integration of some energy dependences.

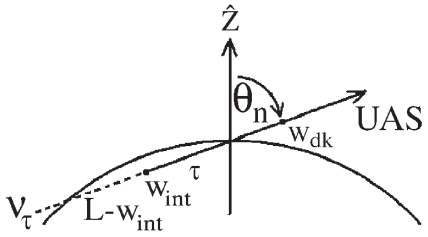

FIG. 2. Coordinates describing UAS.

lepton trajectory; when needed, z will label the distance normal to the Earth's surface, and x and y will label the Earth's tangent plane. The chord length L and the nadir-angle θ_n of the upgoing neutrino trajectory characterize the same degree of freedom, coupled together by the geometric relation $L = 2R_\oplus \cos\theta_n$, where $R_\oplus = 6371$ km is the radius of the Earth.

We follow the calculation of the rate of UAS events as given in Ref. [21], although with some important improvements. The rate is

$$R_{\nu_\tau}(\mathrm{UAS}) = F_{\nu_\tau} \pi A \int_0^{2R_\oplus} \frac{L dL}{2R_\oplus^2} P_{\nu_\tau \to \tau}(L) \otimes P_{\mathrm{dk}}(L), \quad (4)$$

where $P_{\nu_\tau \to \tau}(L)$ is the probability for a ν_τ along a chord of length L in Earth to produce a tau which exits the surface with energy above a given threshold value E^τ_{th}, $P_{\mathrm{dk}}(L)$ is the probability of decay for the tau emerging into the air, and F_{ν_τ} is the ν_τ differential flux in the usual dimensional units of (energy $\cdot$ time $\cdot$ area $\cdot$ steradian)$^{-1}$. The $\otimes$ symbol denotes coupling between the two probabilities, as shown in detail below. In Eq. (4) we have not considered the possibility of the tau decaying inside the Earth, which for the energies of interest in this study is a very good approximation. The detector's field of view (FOV) is $A = \int dx \int dy$. In general, the FOV includes some detector-efficiency weighting for shower identification, as explained in Sec. III. The operator $\pi A \int L dL / 2R_\oplus^2$ is a convenient rewriting of the integrals $\int d\vec{A} \cdot \hat{n} \int d\Omega$, obtained when use is made of the relation $L = 2R_\oplus \cos\theta_n$. The angular dependence of the interaction and decay probabilities are therefore implicit in the L-dependence.

The interaction probability is given by

$$P_{\nu_\tau \to \tau}(L) = \int_0^{\min\{L, w_{\mathrm{th}}\}} \frac{dw_{\mathrm{int}}}{\lambda_\nu(w_{\mathrm{int}})} e^{-\sigma^{\mathrm{CC}}_{\nu N} d_\nu(L, w_{\mathrm{int}})}, \quad (5)$$

where $dw_{\mathrm{int}}/\lambda_\nu$ is the probability for neutrino conversion into tau lepton in the interval $[w_{\mathrm{int}}, w_{\mathrm{int}} + dw_{\mathrm{int}}]$, and the exponential gives the survival probability of the neutrino to reach the interaction point w_{int}. The column density traversed by the neutrino is given by

$$d_\nu = \int_{w_{\mathrm{int}}}^{L} dw \rho_{\mathrm{earth}}(w). \quad (6)$$

If the density ρ_{earth} were a constant, the exponential in Eq. (5) would be simply $e^{-(L - w_{\mathrm{int}})/\lambda_\nu}$, with $\lambda_\nu^{-1} = \sigma^{\mathrm{CC}}_{\nu N} \rho_{\mathrm{earth}}$. Such will be the case if the absorption in the Earth limits chord lengths to just the outer layer of Earth-matter (water or surface rock). The angle of the trajectory above the horizon is related to the chord length as $\sin\theta_{\mathrm{hor}} = L/2R_\oplus$. Setting the chord length equal to the neutrino MFP λ_ν, we get for the typical angle

$$\theta_{\mathrm{hor}} \simeq (2R_\oplus \sigma^{\mathrm{CC}}_{\nu N} \rho_{\mathrm{earth}})^{-1} = 0.28^\circ \times \sigma_{31}^{-1} \left(\frac{\rho_{\mathrm{sr}}}{\rho}\right). \quad (7)$$

A commonly quoted extrapolation for the neutrino CC cross-section is $\sigma_{31} = 0.55$ at 10^{20} eV [11]. Comparisons with the ''critical'' angles delimiting the various density boundaries in the Earth, given in Table IV in the Appendix, then reveals that over ocean, $\sigma^{\mathrm{CC}}_{\nu N} \gtrsim 4 \times 10^{-32}$ cm^2 gives rise to events whose trajectories were dominantly in only water; and over land, $\sigma^{\mathrm{CC}}_{\nu N} \gtrsim 10^{-33}$ cm^2 gives rise to events whose trajectories were dominantly in only surface rock (as opposed to mantle or core). For these events, the Earth density is approximately a constant. We also study smaller cross-sections, for which the density is not constant along the path integral. In the Appendix we present our general calculation of d_ν.

The bound $w_{\mathrm{th}}(\theta_n)$ on the depth of w_{int} integration in Eq. (5) is determined by the requirement that the tau emerge from the Earth with sufficient energy, E^τ_{th}, to produce air showers which trigger the detector apparatus. In general, w_{th} is angle dependent because the density in the Earth is angle dependent. The mean energy of the tau emerging from the Earth is obtained by integrating Eq. (2). The result is[4]

$$E_\tau(w_{\mathrm{int}}) = \frac{E_0}{[1 + \alpha \mathcal{I}(w_{\mathrm{int}})(\frac{E_0}{10^{19}\ \mathrm{eV}})^\alpha]^{1/\alpha}}, \quad (8)$$

where $E_0 = (1 - \langle y \rangle) E_\nu$ is the mean energy of a tau created by an incoming neutrino with incident energy E_ν, and $\langle y \rangle$ is the average inelasticity parameter which we will take as $\langle y \rangle = 0.2$ [32,33]. Thus, we take $E_0 = 0.8 E_\nu$. We define $\mathcal{I}(w_{\mathrm{int}})$ as the dimensionless tau ''opacity'' from point of production to the Earth's surface, *normalized to a tau with* $E = 10^{19}$ eV,

$$\mathcal{I}(w_{\mathrm{int}}) = \int_0^{w_{\mathrm{int}}} dw \beta_{19}(z) \rho_{\mathrm{earth}}(z). \quad (9)$$

This definition allows isolation of the energy dependence of $\beta_\tau(E)$ in a separate factor, evident in Eq. (8). Note that both β_{19} and ρ_{earth} in (9) depend on the Earth's composition (e.g., water versus rock), which in general changes with depth z. For UAS rising from land, there is no

[4]The $\alpha \to 0$ limit of the ln of the denominator in Eq. (8) is easily seen to be $\mathcal{I}$, and so the $\alpha \to 0$ limit of E_τ is $E_0 e^{-\mathcal{I}}$.

z-dependence: $\rho_{\rm earth} = \rho_{\rm sr}$ and $\beta_{19} = 1.0 \times 10^{-6}$ cm^2/g are fixed, and the tau opacity is simply the path length in units of the tau energy-attenuation length at $E_0 = 10^{19}$ eV, $w_{\rm int}/\lambda_\tau(10^{19}\ {\rm eV})$, with $\lambda_\tau(10^{19}\ {\rm eV}) = (\beta_{19}\rho_{\rm sr})^{-1}$. On the other hand, for UAS rising from the oceans, there is a discontinuity at the ocean's bottom: $\rho_{\rm earth}$ comprises two contributions, one from ocean water and the other from the underlying rock. In the Appendix, we show the calculation of I for this case. We will take the depth of the ocean $z_{\rm w}$ to be 3.5 km.

Setting Eq. (8) equal to $E^\tau_{\rm th}$, one obtains

$$I\,(w_{\rm th}(\theta_n)) = \frac{1}{\alpha}\left[\left(\frac{10^{19}\ {\rm eV}}{E^\tau_{\rm th}}\right)^\alpha - \left(\frac{10^{19}\ {\rm eV}}{E_0}\right)^\alpha\right] \qquad (10)$$

as the equation defining the integration maximum $w_{\rm th}$.[5] For UAS rising from land, $\beta_{19}\rho_{\rm sr}$ is constant and the integration and inversion of Eq. (10) to get $w_{\rm th}$ is trivial. For UAS rising from the ocean, the integration and inversion of Eq. (10) to get $w_{\rm th}$ is more complicated, as the path comprises a water and a rock component. Both cases, land and ocean, are dealt with in the Appendix.

The decay probability is

$$P_{\rm dk}(L) = \int_0^\infty \frac{dw_{\rm dk}}{\tau}\, e^{-w_{\rm dk}/\tau} \qquad (11)$$

with the tau lifetime in the lab frame given by

$$\tau = \frac{E_\tau}{m_\tau}\tau_{\rm RF} = \frac{392(E_\nu/10^{19}\ {\rm eV})\ {\rm km}}{[1 + \alpha I(w_{\rm int})(0.8E_\nu/10^{19}\ {\rm eV})^\alpha]^{1/\alpha}}, \qquad (12)$$

where $\tau_{\rm RF}$ is the rest-frame value of the tau lifetime. The numerical expression in Eq. (12) properly includes the 0.8 mean factor for energy transfer between the incident ν_τ and the τ. We remind the reader that, for the simple case of UAS over rock, the opacity is just $I = \beta_{19}\rho_{\rm sr}w_{\rm int}$. The more complicated case for UAS over oceans is dealt with in the Appendix.

When the tau decays, it has a 64% branching probability to decay to ν_τ + hadrons. For an unpolarized tau, $\sim 2/3$ of the energy goes into the hadrons, and therefore into the shower. Accordingly, for this mode we take the relation between tau and shower energies to be $\frac{2}{3}E^\tau = E^{\rm sh}$. We define $E^{\rm sh}_{\rm th}$ to be the minimum-energy trigger for the detector. Thus, we have the threshold relation $E^\tau_{\rm th} = \frac{3}{2}E^{\rm sh}_{\rm th}$. The tau also has 18% branching probabilities each into $\nu + \bar\nu + e$ and $\nu + \bar\nu + \mu$. The electronic mode immediately creates an electromagnetic shower with $\sim 1/3$ of the tau energy, on average. So for the electronic mode we take the relation between thresholds to be $E^\tau_{\rm th} = 3E^{\rm sh}_{\rm th}$. The muonic mode is ignorable, for the decay length of the muon exceeds the distance to the ground. In our calculation of the UAS acceptance, we will weight each tau decay with 64% for the hadron mode where $E^{\rm sh}_{\rm th} = \frac{2}{3}E^\tau_{\rm th}$, and 18% for the electron mode where $E^{\rm sh}_{\rm th} = \frac{1}{3}E^\tau_{\rm th}$; the remaining 18% is the unobservable muon mode.[6]

The two integrals in Eqs. (5) and (11) are coupled via the $w_{\rm int}$-dependent lifetime of the tau. When we later introduce constraints due to cloud covering, we will see further coupling among the integration variables. The exponential in Eq. (11) describes the survival probability of the upgoing tau lepton to reach the decay point $w_{\rm dk}$. There is some probability for the tau to decay inside the Earth in the interval $[0, w_{\rm int}]$, but as we mentioned above it is negligibly small in the energy range of interest. There is regeneration of tau neutrinos over the whole Earth due to the tau production and decay chain, but the regenerated taus with their lower energy contribute negligibly to the high-energy sample discussed here and so are not included.

In practice, a sufficient column density of air beyond the tau decay point $w_{\rm dk}$ is required such that the decay products fully develop into a shower. This requirement will cutoff the integration in Eq. (11), and provide an L-dependence (or $\cos\theta_n$-dependence) to $P_{\rm dk}$. In the original study [21], a simple analytic result for the decay integral (11) was obtained by invoking certain approximations. The tau lifetime was taken to be a constant over the energy range of interest, and the integral was cutoff at the scale height of the atmosphere, $h = 8$ km. With these approximations, one obtains for the decay integral $P_{\rm dk} = 1 - e^{-h/(\tau\cos\theta_n)} = 1 - e^{-2R_\oplus h/L\tau}$. Also, the air-shower rate per incident ν_τ was computed analytically for the case where the angle above the horizon satisfies $\theta_{\rm hor} \gg (10^{17}\ {\rm eV}/E_\tau)$ degrees so that $P_{\rm dk} \approx 2R_\oplus h/L\tau$. In this work, we do not adopt these approximations. Here, the implicit energy dependence of the UAS rate in Eq. (4) arises from the energy dependences of $w_{\rm th}$, λ_ν, and τ, as well as from the differential flux F_{ν_τ}. We will present results for the full nested integrals of Eq. (4).

B. Horizontal air-showers (HAS)

We now turn to the derivation of the HAS event rate. Neutrino-induced air-showers come in several topologies [6]. All three neutrino flavors contribute equally to the neutral current (NC) events, but these transfer on average only 20% of the incident energy to the shower. Furthermore, the NC interaction rate is smaller, about

[5] Writing $(E^\tau_{\rm th})^{-\alpha}$ as $e^{-\alpha \ln E^\tau_{\rm th}}$, and similarly for $E_0^{-\alpha}$, one readily finds the $\alpha \to 0$ limit of Eq. (10) to be $I(w_{\rm th}(\theta_z)) = \ln(E_0/E^\tau_{\rm th})$.

[6] The tau is 100% polarized (to order m_τ/E_τ) at production in the Earth. It is possible that even after multiscattering in the Earth (mainly due to photonuclear interactions), the tau retains some of its initial polarization. If so, then the decay particle with helicity opposite to that of the tau is softer on average. The net result is slightly more energy transferred to the electromagnetic shower, and slightly less energy transferred to the hadronic shower [34].

44%, than the charged-current (CC) rate. Among the CC events, the leading muon and tau from incident ν_μ and ν_τ, respectively, are not visible in the air (unless the tau decays in a "double-bang" event). In the CC process, only 20% of the incident energy is transferred to the visible shower. For a ν_e-initiated CC event, the produced electron contributes electromagnetically to the shower, so the full incident energy converts to shower energy. In summary, about one event in four (the ν_e CC interaction) will transfer 100% of the incident energy to the shower, while three events in four will transfer $\sim$20% of the energy.[7]

To be definite, we assume a ν_e CC interaction in what follows. We label the spatial axes as z for vertical upward and x and y for the directions tangent to the Earth's surface; curvature of the Earth's surface may be neglected for HAS. It is useful to consider first a parallel neutrino flux perpendicular to $\hat{x}$, incident with a zenith angle θ_z, as illustrated in the projections of Figs. 3 and 4. The horizontal air-shower probability is

$$R_{\nu_e}(\mathrm{HAS}) = F_{\nu_e}\int d\Omega \int \sigma_{\nu N}^{\mathrm{CC}}\rho_{\mathrm{atm}}(\vec{r}_{\mathrm{int}})d^3r_{\mathrm{int}} = F_{\nu_e}2\pi A\sigma_{\nu N}^{\mathrm{CC}}\rho_{\mathrm{atm}}(0)\int d\cos\theta_z \int e^{-z_{\mathrm{int}}/h}dz_{\mathrm{int}}, \tag{13}$$

where $\vec{r}_{\mathrm{int}}$ is the point of interaction, $A = \int dx \int dy$ again, and the second expression follows from the first when the atmospheric density function

$$\rho_{\mathrm{atm}}(z) = \rho_{\mathrm{atm}}(0)e^{-z/h} \tag{14}$$

is inserted. We set the scale height $h = 8$ km. The factor of $\int d\Omega = 2\pi \int d\cos\theta_z$ in Eq. (13) rotates the incident flux, initially assumed to be parallel and now assumed to be isotropic, over the full sky.

In principle, we should include the curvature of the Earth's surface in assessing the vertical height z in $\rho(z)$ along the developing shower. In practice, this is unnecessary as long as the shower length is a small fraction of the Earth's radius, as is the case here (we will return to the curvature issue later in the discussion of UAS events).

The HAS event rate scales linearly with the cross-section $\sigma_{\nu N}^{\mathrm{CC}}$. This is because the absorption probability of the neutrino in the atmosphere is negligibly small. The natural scales of atmospheric column density are the vertical density

$$d_{\mathrm{vert}} \equiv \int_0^\infty dz\rho_{\mathrm{atm}}(z) = h\rho_{\mathrm{atm}}(0) = 1030\ \mathrm{g/cm^2}, \tag{15}$$

and the horizontal density

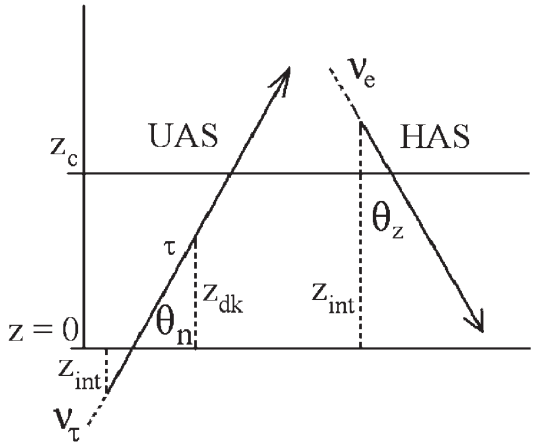

FIG. 3. Lateral snapshot of UAS and HAS; z labels vertical altitudes and depths.

$$d_{\mathrm{hor}} = \int_0^\infty dx\rho_{\mathrm{atm}}(z = \sqrt{R_\oplus^2 + x^2} - R_\oplus) \approx d_{\mathrm{vert}}\int_0^\infty du e^{-u^2h/2R_\oplus} = \sqrt{\pi R_\oplus/2h}\,d_{\mathrm{vert}} = 36d_{\mathrm{vert}}. \tag{16}$$

In terms of the latter, the neutrino absorption probability in the atmosphere is

$$P(\nu - \text{air absorption}) = \sigma_{\nu N}^{\mathrm{CC}}N_A d_{\mathrm{hor}}\left(\frac{d}{d_{\mathrm{hor}}}\right) = 2\times 10^{-3}\sigma_{31}\left(\frac{d}{d_{\mathrm{hor}}}\right) \tag{17}$$

where $d \le d_{\mathrm{hor}}$ is the column density of the neutrino's trajectory in the atmosphere. Thus, for $\sigma_{\nu N}^{\mathrm{CC}} \lesssim 10^{-29}$ cm^2, atmospheric absorption is negligible even for horizontal neutrinos, and so the neutrino interaction rate scales linearly with $\sigma_{\nu N}^{\mathrm{CC}}$.

Further restrictions on the integration variables result from further assumptions for detector efficiencies. Let us assume that the air-shower must originate in the detector FOV of area A. Then the straightforward integration of Eq. (13) gives

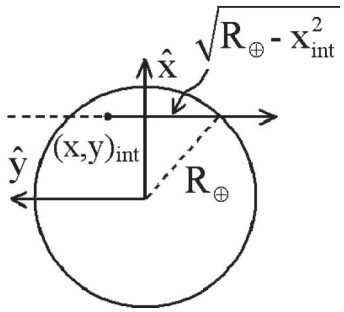

FIG. 4. Overhead snapshot of the event projected onto the field of view (FOV).

[7]If the incident neutrino spectrum is falling as a power, then *at fixed energy* the ν_e CC events dominate the total rate.

$$R_{\nu_e}(\mathrm{HAS}) = 2\pi A F_{\nu_e} h \sigma^{\mathrm{CC}}_{\nu N} \rho_{\mathrm{atm}}(0). \quad (18)$$

The value $h\sigma^{\mathrm{CC}}_{\nu N}\rho_{\mathrm{atm}}(0) = 0.62 \times 10^{-4}\sigma_{31}$ sets the scale for the interaction probability in the atmosphere per incident neutrino. The resulting value of the acceptance[8] is $\mathcal{A}cc \equiv R_{\nu_e}(\mathrm{HAS})/F_{\nu_e} = 2\pi A h \sigma^{\mathrm{CC}}_{\nu N}\rho_{\mathrm{atm}}(0) = 3.9\sigma_{31}(\frac{A}{10^4\ \mathrm{km}^2})\ \mathrm{km}^2\,\mathrm{sr}$. This value suggests that wide-angle, large-area detectors exceeding 10^4 km^2 sr, and cosmic neutrino fluxes exceeding $1/\mathrm{km}^2\,\mathrm{sr\,yr}$, are needed for event collection. Put another way, full sky coverage of an air mass of $\sim 10^5$ km$^2 \times h\rho(0) \sim$ teraton is required.

III. CONSTRAINTS FROM DEVELOPMENT AND IDENTIFICATION OF SHOWERS

In this section we address conditions for the showers to be observable. First of all, shower detection will require that, within the FOV, the length of the shower track projected on a plane tangent to the Earth's surface (as would be seen from far above or far below) exceeds some minimum length, l_{min}. Space-based observatories are far above the Earth, and so view the atmosphere as a two-dimensional plane. For ground-based observatories, tangential projections may not be the optimum way to describe the FOV constraint, but we use it as a guide.

In addition to the projected length constraint, there are three ''shower-development'' constraints to be applied to the events. A minimum column density, d_{min}, beyond the point of shower initiation is required for the shower to develop in brightness. On the other hand, after a maximum column density, d_{max}, the shower particles are below threshold for further excitation of the N_2 molecules which provide the observable fluorescence signal. We therefore terminate showers at d_{max}, which implies a finite length for the visible shower.

While the requirements of minimum projected length, and minimum and maximum shower column densities are correlated, no two of them implies the third. Some reflection on the θ and z dependences of the varying densities and projected lengths reveals that this is so.

Finally, the fluorescent emission per unit length of the shower will decline exponentially with the air density at altitude. At $z = 2h$, the fluorescent emission is down to $e^{-2} = 14\%$ of that at sea level. At $z = 3h(4h)$, it is down to 5% (2%) of that at sea level. Atmospheric absorption of the emitted fluorescence also affects the signal. This absorption is thought to scale roughly as the atmospheric density, up to about 20 km [35]. Thus, it turns out that the fluorescence signal could roughly be taken as constant between zero and 20 km. Accordingly, we will take $z_{\mathrm{thin}} = 3h = 24$ km as the ''too-thin'' altitude beyond which the signal becomes imperceptible.

Thus, there are four constraints that render the shower observable. These are the l_{min}, d_{min}, d_{max}, and ''too-thin'' (or z_{thin}) conditions. The values which we choose for these parameters are listed in Table II. The choice for the z_{thin} value was discussed and motivated above. The d_{min} and d_{max} choices are inferred from the observed longitudinal development profiles of ultrahigh-energy cosmic-ray showers (the famous Fly's Eye event at energy 3×10^{20} eV provides a splendid example [5]). Showers at 300–400 g/cm^2 of column density (also called ''atmospheric depth'' or ''slant depth'') comprise tens of billions of electrons, with a brightness roughly 10% of shower maximum. The electrons in showers at $\gtrsim 1200$ g/cm^2 are ranging out, reducing significantly the shower brightness. We assign a relatively small value to l_{min} to maximize the observable event rate. For the EUSO experiment, each pixel is a map of a square kilometer of the Earth's surface [35]. Thus, an l_{min} of 10 km corresponds to a signal in ten contiguous pixels. The background for ten contiguous pixels should be small. With ten pixels, the angular reconstruction of the event direction is roughly 1/10 rad ($\sim$ 5 deg). With a cloud layer a smaller l_{min} value for event triggering may be needed. With an l_{min} of 5 km, the signal-to-noise should still be acceptable. For $l_{\mathrm{min}} = 5$ km, the angular reconstruction is reduced to 1/5 rad ($\sim$ 10 deg), though.

A. Effective area

Let us describe the projected length l_{min} constraint, and the d_{min} and d_{max} constraints in the general case. Consider a detector with a FOV characterized by a radius R_{FOV}, i.e., (see Fig. 4)

$$x^2 + y^2 \leq R^2_{\mathrm{FOV}}. \quad (19)$$

We define the y-z plane to be the shower plane. A shower produced with initial coordinates (x, y, z) cannot have a visible projected length larger than the chord length $y + \sqrt{R^2_{\mathrm{FOV}} - x^2}$ in the FOV. However, the projected length may be smaller, for three reasons. The first is that the shower must develop and brighten before becoming visible. This requires traversing the column density d_{min}. The second reason is that the shower may hit the ground (attain the ''too-thin'' altitude) before reaching the far boundary of the FOV in the case of HAS (UAS). Thirdly, the shower may extinguish before reaching the far boundary of the FOV. Extinction occurs when the traversed column density attains the value d_{max}. For HAS (UAS), we label the upper altitude where the shower becomes visible (extinguishes or strikes the ''too-thin'' altitude) as z_U, and the lower altitude where the shower extinguishes or strikes the ground (becomes visible) as z_L. We will use the HAS or UAS label on

[8] One may also write the acceptance as $2\pi A(h/\lambda_\nu)$, where $\lambda_\nu^{-1} = \sigma^{\mathrm{CC}}_{\nu N}\rho_{\mathrm{atm}}(0)$ is the neutrino MFP. This expression is the $\lambda_\nu \gg h$ limit of $\mathcal{A}cc = 2\pi A(1 - e^{-h/\lambda_\nu})$. In this latter form, one sees the acceptance saturating its geometric value of $2\pi A$ in the strong cross-section limit.

z_U and z_L to distinguish between these altitudes in the two cases. The altitudes z_B and z_E, to be defined shortly, will also carry a HAS or UAS label. For brevity, we will sometimes omit the HAS and UAS labels when it is clear from the context which label applies.

From the above shower-development considerations, the visible shower length projected on the Earth's surface is $(z_U - z_L)\tan\theta$. Collecting the remarks above, the projected air-shower length within the FOV of the detector is then

$$l_{\rm FOV} = \min\{[z_U - z_L]\tan\theta,\, y + \sqrt{R_{\rm FOV}^2 - x^2}\}. \tag{20}$$

We will discuss the maximum and minimum altitude values z_U and z_L for each type of shower in the following subsections.

For the projected length in the FOV to exceed some minimum length, $l_{\rm min}$, we infer from Eq. (20) the set of conditions

$$y + \sqrt{R_{\rm FOV}^2 - x^2} \geq l_{\rm min}, \tag{21}$$

$$[z_U - z_L]\tan\theta \geq l_{\rm min}. \tag{22}$$

After algebraic manipulation of constraints (19) and (21), the area integral $\int dx \int dy$ is easily done, yielding

$$A = \pi R_{\rm FOV}^2\left(\frac{\arcsin\eta - \eta\sqrt{1-\eta^2}}{\pi/2}\right), \tag{23}$$

where

$$\eta \equiv \sqrt{1 - \frac{l_{\rm min}^2}{4R_{\rm FOV}^2}} \tag{24}$$

is nearly one in a large-area experiment. This is then the constraint-modified meaning of A. Since the arguments leading to it apply equally to the HAS and UAS geometry, the result in Eq. (23) applies in both rates, Eqs. (4) and (13). We note that, for $l_{\rm min} \ll 2R_{\rm FOV}$, the expression in parenthesis in (23) is nearly unity, with an expansion

$$1 - \frac{3}{\pi}\left(\frac{l_{\rm min}}{2R_{\rm FOV}}\right) + \mathcal{O}\left(\frac{l_{\rm min}}{2R_{\rm FOV}}\right)^3. \tag{25}$$

Thus, with $l_{\rm min} \ll 2R_{\rm FOV}$, the constrained area is just the geometric area.

B. Four constraints for HAS

In this subsection we develop the $l_{\rm min}$, $d_{\rm min}$, $d_{\rm max}$, and "too-thin" (or $z_{\rm thin}$) constraints for HAS.

The "too-thin" constraint at high altitude is simple. It effectively implies ($w_{\rm int} = z_{\rm int}/\cos\theta_z$)

$$z_{\rm ground} \leq z_{\rm int} \leq z_{\rm thin}, \tag{26}$$

where $z_{\rm ground} = 0$ labels the altitude of the ground at sea level. We will retain the symbol $z_{\rm ground}$ even though it is zero in the present context. Retaining $z_{\rm ground}$ will be useful for substitutions in later sections where we include a cloud layer.

The projected track length condition, given in Eq. (22), is

$$[z_U({\rm HAS}) - z_L({\rm HAS})]\tan\theta_z \geq l_{\rm min}. \tag{27}$$

Now we consider the calculations of the maximum and minimum visible-shower altitudes, z_U(HAS) and z_L(HAS), respectively, which enter this formula. The column densities of the HAS showers evolved from initial altitude $z_{\rm int}$ to the lower altitude z are given by

$$\begin{aligned} d({\rm HAS}; z) &= \int_z^{z_{\rm int}} \frac{dz}{\cos\theta_z}\rho_{\rm atm}(z) \\ &= \frac{d_{\rm vert}}{\cos\theta_z}(e^{-z/h} - e^{-z_{\rm int}/h}). \end{aligned} \tag{28}$$

The evaluated integral uses the exponential decrease of the atmospheric density with increasing altitude and the definition $d_{\rm vert} = h\rho_{\rm atm}(0)$. Equating $d({\rm HAS}; z)$ to $d_{\rm min}$, we get the altitude where the shower first becomes visibly bright. We call this altitude z_B(HAS). Positivity of the integrand ensures that $z_B < z_{\rm int}$ for any atmospheric density profile. Implicitly, z_B(HAS) is given by

$$e^{-z_B({\rm HAS})/h} - e^{-z_{\rm int}/h} = \frac{d_{\rm min}}{d_{\rm vert}}\cos\theta_z. \tag{29}$$

Explicit solutions for z_B(HAS) as a function of $z_{\rm int}$ and vice versa are

$$\begin{aligned} z_B({\rm HAS}) &= -h\ln\left[e^{-z_{\rm int}/h} + \frac{d_{\rm min}}{d_{\rm vert}}\cos\theta_z\right]; \\ z_{\rm int} &= -h\ln\left[e^{-z_B({\rm HAS})/h} - \frac{d_{\rm min}}{d_{\rm vert}}\cos\theta_z\right]. \end{aligned} \tag{30}$$

A shower becomes visible above the ground level only if $z_B > z_{\rm ground}$. From Eq. (29), the condition $z_B > z_{\rm ground}$ implies

$$z_{\rm int} > -h\ln\left[e^{-z_{\rm ground}/h} - \frac{d_{\rm min}}{d_{\rm vert}}\cos\theta_z\right]. \tag{31}$$

Although this condition ensures a visible shower above the ground, it allows the visible length to be arbitrarily small. The requirement of a visible projected length in excess of $l_{\rm min}$ will lead to a stronger constraint, presented below in Eq. (38). However, Eq. (31) is useful in that it implies an absolute limit on the shower direction. Since $z_{\rm int}$ is less than $z_{\rm thin}$ by construction [Eq. (26)], the limit is

$$\cos\theta_z \leq \frac{d_{\rm vert}}{d_{\rm min}}(e^{-z_{\rm ground}/h} - e^{-z_{\rm thin}/h}) \approx \frac{d_{\rm vert}}{d_{\rm min}}. \tag{32}$$

There is no absolute restriction on angle from the $d_{\rm min}$ constraint if $d_{\rm min}$ is less than $d_{\rm vert} = 1030\ {\rm g/cm^2}$, since then even a vertical shower traverses enough column den-

sity to brighten. We will take 400 g/cm^2 as our standard value for $d_{\rm min}$.

The calculation of z_L(HAS) proceeds analogously to the calculation of z_U(HAS). Setting the column density d(HAS; z) equal to $d_{\rm max}$, we get the altitude where the shower extinguishes. We call this altitude z_E(HAS). Implicitly, z_E(HAS) is given by

$$e^{-z_E({\rm HAS})/h} - e^{-z_{\rm int}/h} = \frac{d_{\rm max}}{d_{\rm vert}} \cos\theta_z. \tag{33}$$

The left-hand side (LHS) of Eq. (33) is maximized by setting z_E(HAS) equal to $z_{\rm ground}$ and $z_{\rm int}$ to $z_{\rm thin}$. If the right-hand side (RHS) exceeds this maximum value, then for any $z_{\rm int}$ the total column density remains less than $d_{\rm max}$, the shower does not extinguish, and there is effectively no $d_{\rm max}$ constraint. So, for more-vertical showers obeying

$$\cos\theta_z \geq \frac{d_{\rm vert}}{d_{\rm max}} (e^{-z_{\rm ground}/h} - e^{-z_{\rm thin}/h}) \equiv \cos\hat{\theta}_z, \tag{34}$$

the shower hits the ground before extinction and thus, we have z_L(HAS) = $z_{\rm ground}$.

On the other hand, when $\cos\theta_z < \cos\hat{\theta}_z$, then whether or not the shower extinguishes before striking the ground depends on the height in the atmosphere at which the shower originated, i.e., on $z_{\rm int}$. Solving Eq. (33) explicitly for z_E(HAS) as a function of $z_{\rm int}$ and vice versa, one gets

$$\begin{aligned} z_E({\rm HAS}) &= -h \ln\left[e^{-z_{\rm int}/h} + \frac{d_{\rm max}}{d_{\rm vert}} \cos\theta_z \right]; \\ z_{\rm int} &= -h \ln\left[e^{-z_E({\rm HAS})/h} - \frac{d_{\rm max}}{d_{\rm vert}} \cos\theta_z \right]. \end{aligned} \tag{35}$$

The shower strikes the ground if $z_E \leq z_{\rm ground}$, and extinguishes if $z_E > z_{\rm ground}$. The critical value is $z_E = z_{\rm ground}$. At this critical value, (35) gives

$$z_{\rm int} = -h \ln\left[e^{-z_{\rm ground}/h} - \frac{d_{\rm max}}{d_{\rm vert}} \cos\theta_z \right] \equiv \hat{z}({\rm HAS}). \tag{36}$$

Thus we have two cases: for $z_{\rm int} \leq \hat{z}$(HAS), the shower strikes the ground and the minimum altitude is $z_L = z_{\rm ground}$; while for $z_{\rm int} > \hat{z}$(HAS) (which implies $\cos\theta_z < \cos\hat{\theta}_z$ because $z_{\rm int} < z_{\rm thin}$ by construction), the shower extinguishes above the ground and $z_L = z_E$(HAS). The latter case corresponds to Eq. (35) having a real-valued solution in the physical interval $[z_{\rm ground}, z_{\rm thin}]$, whereas the former case corresponds to no such solution for Eq. (35). The high altitude z_U(HAS) is where the shower begins its visible track length. Accordingly, we set z_U(HAS) = z_B(HAS) in the $l_{\rm min}$ constraint for both cases, where z_B(HAS) is given in Eq. (30).

For $z_{\rm int} > \hat{z}$(HAS), the shower extinguishes and we substitute z_U(HAS) = z_B(HAS) and z_L(HAS) = z_E(HAS), given in Eqs. (30) and (35), respectively, into Eq. (27). After a bit of algebra, one finds that the resulting $l_{\rm min}$ constraint can be expressed as

$$z_{\rm int} > -h \ln\left[\frac{\cos\theta_z}{d_{\rm vert}} \left(\frac{d_{\rm max} - d_{\rm min} e^{l_{\rm min}/(h\tan\theta_z)}}{e^{l_{\rm min}/(h\tan\theta_z)} - 1} \right) \right]. \tag{37}$$

Real values of $z_{\rm int}$ in the interval $[\hat{z}({\rm HAS}), z_{\rm thin}]$ which satisfy this equation, if any, satisfy all four constraints for $\cos\theta_z < \cos\hat{\theta}_z$, and so contribute to the integral for the observable event rate.

For the other case, where $z_{\rm int} < \hat{z}$(HAS), the shower strikes the ground. We have z_U(HAS) = z_B(HAS), the latter given in Eq. (30), and z_L(HAS) = $z_{\rm ground}$. Inputting these expressions into Eq. (27), one finds an explicit expression for the $l_{\rm min}$ constraint,

$$z_{\rm int} > -h \ln\left[e^{-(l_{\rm min}/(\tan\theta_z) + z_{\rm ground})/h} - \frac{d_{\rm min}}{d_{\rm vert}} \cos\theta_z \right]. \tag{38}$$

This constraint ensures a visible projected length exceeding $l_{\rm min}$. It replaces the constraint of Eq. (31), which ensured only a nonzero visible track length. Of course, in the limit $l_{\rm min} = 0$, the two constraints are identical. Real values of $z_{\rm int}$ in the interval $[z_{\rm ground}, z_{\rm thin}]$ for $\cos\theta_z \geq \cos\hat{\theta}_z$, or in the interval $[z_{\rm ground}, \hat{z}({\rm HAS})]$ for $\cos\theta_z < \cos\hat{\theta}_z$, which satisfy this equation, if any, satisfy all four constraints and so contribute to the integral for the observable event rate.

To summarize the HAS rate formulas in the absence of cloud cover, we have the general rate equation, Eq. (13), with the area given in Eq. (23), and the ''too-thin'' constraint in Eq. (26). There are two alternate ways to express the $d_{\rm min}$, $d_{\rm max}$, and $l_{\rm min}$ constraints. The first way is to define the boundaries of $(z_{\rm int}, \theta_z)$-integration physically but implicitly. This is done with Eq. (27) implementing the $l_{\rm min}$ constraint, where z_U(HAS) = z_B(HAS) implements the $d_{\rm min}$ constraint with z_B(HAS) given in Eq. (30), and z_L(HAS) = max$\{z_{\rm ground}, z_E({\rm HAS})\}$ implements the $d_{\rm max}$ constraint with z_E(HAS) given in Eq. (35). If Eq. (35) has no real-valued solutions in the interval $[z_{\rm ground}, z_{\rm thin}]$, then z_L(HAS) = $z_{\rm ground}$. The value of $z_{\rm ground}$ is zero (in the absence of clouds).

The alternative way to express the $d_{\rm min}$, $d_{\rm max}$, and $l_{\rm min}$ constraints is to solve the constraints of the first approach for explicit boundaries on the $(z_{\rm int}, \theta_z)$-integration. The results of this approach bifurcate, depending on whether the shower extinguishes, or the shower strikes the ground. For the case where the shower extinguishes, the boundaries are given by $z_{\rm int} > \hat{z}$(HAS), with $\hat{z}$(HAS) defined in Eq. (36), and by Eq. (37). For the case where the shower strikes the ground, the boundaries are given by $z_{\rm int} < \hat{z}$(HAS), and by Eq. (38). *A priori*, there is no guarantee that Eqs. (37) and (38) have real-valued solutions in the physical region of $z_{\rm int}$.

C. Four constraints for UAS

The calculation of the $l_{\rm min}$, $d_{\rm min}$, $d_{\rm max}$, and ''too-thin'' (or $z_{\rm thin}$) constraints for UAS events proceeds analogously

to the calculation for HAS events. The ''too-thin'' altitude constraint is again

$$z_{\rm ground} \leq z_{\rm dk} \leq z_{\rm thin}. \tag{39}$$

At sea level, $z_{\rm ground} = 0$. The projected track length condition for UAS events, analogous to Eq. (27) for HAS events, is

$$[z_U({\rm UAS}) - z_L({\rm UAS})]\tan\theta_n \geq l_{\rm min}. \tag{40}$$

The values of z_U(UAS) and z_L(UAS) differ from z_U(HAS) and z_L(HAS). To calculate them, we turn to calculations of UAS column densities, given by

$$\begin{aligned} d({\rm UAS}; z) &= \int_{z_{\rm dk}}^{z} \frac{dz}{\cos\theta_n}\rho_{\rm atm}(z) \\ &= \frac{d_{\rm vert}}{\cos\theta_n}(e^{-z_{\rm dk}/h} - e^{-z/h}). \end{aligned} \tag{41}$$

Setting this equal to $d_{\rm min}$ defines implicitly the brightness altitude z_B(UAS):

$$e^{-z_{\rm dk}/h} - e^{-z_B({\rm UAS})/h} = \frac{d_{\rm min}}{d_{\rm vert}}\cos\theta_n. \tag{42}$$

Solving this equation explicitly for z_B(UAS) as a function of $z_{\rm dk}$ and vice versa, one gets

$$\begin{aligned} z_B({\rm UAS}) &= -h\ln\left[e^{-z_{\rm dk}/h} - \frac{d_{\rm min}}{d_{\rm vert}}\cos\theta_n\right]; \\ z_{\rm dk} &= -h\ln\left[\frac{d_{\rm min}}{d_{\rm vert}}\cos\theta_n + e^{-z_B({\rm UAS})/h}\right]. \end{aligned} \tag{43}$$

We require that $z_B({\rm UAS}) < z_{\rm thin}$; otherwise, the shower invisibly disappears into thin air. From Eq. (43), the condition $z_B({\rm UAS}) < z_{\rm thin}$ can be written

$$z_{\rm dk} \leq -h\ln\left[\frac{d_{\rm min}}{d_{\rm vert}}\cos\theta_n + e^{-z_{\rm thin}/h}\right]. \tag{44}$$

This condition ensures visibility of the shower, but with a visible length arbitrarily small. The requirement of a visible projected length in excess of $l_{\rm min}$ will lead to a stronger constraint, presented in Eq. (50) below. Positivity of $z_{\rm dk}$ and Eq. (44) lead to the same angular constraint for $\cos\theta_z$ as was found for HAS's $\cos\theta_n$ in Eq. (32).

Setting $d({\rm UAS}; z)$ equal to $d_{\rm max}$, we get the high altitude z_E(UAS) where the UAS shower extinguishes. Implicitly, this highest visible altitude is given by

$$e^{-z_{\rm dk}/h} - e^{-z_E({\rm UAS})/h} = \frac{d_{\rm max}}{d_{\rm vert}}\cos\theta_n. \tag{45}$$

The LHS of Eq. (45) is maximized by setting $z_{\rm dk}$ equal to $z_{\rm ground}$ and z_E(UAS) to $z_{\rm thin}$. If the RHS exceeds this maximum value, then for any $z_{\rm dk}$ the total column density remains less than $d_{\rm max}$, the shower does not extinguish, and there is effectively no $d_{\rm max}$ constraint. So, for more-vertical showers obeying

$$\cos\theta_n \geq \frac{d_{\rm vert}}{d_{\rm max}}(e^{-z_{\rm ground}/h} - e^{-z_{\rm thin}/h}) \equiv \cos\hat{\theta}_n, \tag{46}$$

we have $z_U({\rm UAS}) = z_{\rm thin}$.

On the other hand, when $\cos\theta_n < \cos\hat{\theta}_n$, then whether or not the shower extinguishes before reaching the ''too-thin'' boundary depends on the height in the atmosphere at which the shower originated, i.e., on $z_{\rm dk}$. Solving Eq. (45) explicitly for z_E(UAS) as a function of $z_{\rm dk}$ and vice versa, one gets

$$\begin{aligned} z_E({\rm UAS}) &= -h\ln\left[e^{-z_{\rm dk}/h} - \frac{d_{\rm max}}{d_{\rm vert}}\cos\theta_n\right]; \\ z_{\rm dk} &= -h\ln\left[\frac{d_{\rm max}}{d_{\rm vert}}\cos\theta_n + e^{-z_E({\rm UAS})/h}\right]. \end{aligned} \tag{47}$$

The shower extinguishes if $z_E({\rm UAS}) < z_{\rm thin}$, and hits the ''too-thin'' boundary if $z_E({\rm UAS}) \geq z_{\rm thin}$. The critical value is $z_E({\rm UAS}) = z_{\rm thin}$. Inputting this critical z_E into Eq. (47), one finds a critical value for the decay altitude:

$$z_{\rm dk} = -h\ln\left[\frac{d_{\rm max}}{d_{\rm vert}}\cos\theta_n + e^{-z_{\rm thin}/h}\right] \equiv \hat{z}({\rm UAS}). \tag{48}$$

For $z_{\rm dk} < \hat{z}$(UAS), the shower attains the ''length'' $d_{\rm max}$ and extinguishes, whereas for $z_{\rm dk} > \hat{z}$(UAS), the shower reaches the ''too-thin'' boundary $z_{\rm thin}$ without extinction.

For $z_{\rm dk} < \hat{z}$(UAS), the shower extinguishes and so $z_U({\rm UAS}) = z_E({\rm UAS})$. Substituting this [Eq. (47)] and $z_L({\rm UAS}) = z_B({\rm UAS})$ from Eq. (43) into the $l_{\rm min}$ constraint Eq. (40) leads to an explicit expression for the $l_{\rm min}$ constraint:

$$z_{\rm dk} \geq -h\ln\left[\frac{\cos\theta_n}{d_{\rm vert}}\left(\frac{d_{\rm max}e^{l_{\rm min}/(h\tan\theta_n)} - d_{\rm min}}{e^{l_{\rm min}/(h\tan\theta_n)} - 1}\right)\right] \equiv z_{<}. \tag{49}$$

This limit, like the analogous one for HAS in Eq. (37), forces the shower initiation to occur at a higher altitude where the air is thinner, and therefore, for fixed $d_{\rm max}$, the shower and its projection are longer. There is no $d_{\rm min}$ constraint for a shower that saturates $d_{\rm max}$.

For $z_{\rm dk} \geq \hat{z}$(UAS), the shower reaches $z_{\rm thin}$ without extinction. Therefore, there is no $d_{\rm max}$ constraint and we set $z_U({\rm UAS}) = z_{\rm thin}$. Substituting this and $z_L({\rm UAS}) = z_B({\rm UAS})$ into the $l_{\rm min}$ constraint Eq. (40), we find the following explicit expression for the $l_{\rm min}$ constraint:

$$z_{\rm dk} < -h\ln\left[e^{(l_{\rm min}/(\tan\theta_n) - z_{\rm thin})/h} + \frac{d_{\rm min}}{d_{\rm vert}}\cos\theta_n\right] \equiv z_{>}. \tag{50}$$

For this class of showers which reach the ''too-thin'' boundary, this upper bound on $z_{\rm dk}$ ensures a visible projected length exceeding $l_{\rm min}$. It supersedes the constraint of Eq. (44), which ensured only a visible track of nonzero length. Of course, in the limit $l_{\rm min} = 0$, the two conditions are identical.

The essence of the $l_{\rm min}$ constraint is that the shower must have sufficient nadir angle to attain a minimum horizontal projection. Thus, there is a critical angle $\theta_n^{\rm crit}$ for which the conditions of Eqs. (49) and (50) collapse to $z_< = \hat{z}({\rm UAS}) = z_>$. For nadir angles smaller than $\theta_n^{\rm crit}$, i.e., for $\cos\theta_n > \cos\theta_n^{\rm crit}$, there are no observable events. Setting $z_< = \hat{z}({\rm UAS}) = z_>$, one finds that this critical angle is given implicitly by

$$z_{\rm thin} = -h \ln\left[\frac{d_{\rm max} - d_{\rm min}}{d_{\rm vert}} \frac{\cos\theta_n^{\rm crit}}{e^{l_{\rm min}/(h\tan\theta_n^{\rm crit})} - 1}\right]. \quad (51)$$

This critical angle encapsulates a relatively weak constraint in the cloudless case. However, it will become a strong constraint when we consider cloudy skies.

To summarize the UAS rate formulas in the absence of cloud cover, we have the general rate equation, Eq. (4), with inputs from Eqs. (5), (6), (8)–(12), and (23), and the ''too-thin'' constraint in Eq. (39). As was the case for the HAS events, there are two alternative ways to express the $d_{\rm min}$, $d_{\rm max}$, and $l_{\rm min}$ constraints for UAS events. The physical but implicit approach bounds the $(z_{\rm dk}, \theta_n)$-integration with Eq. (40) implementing the $l_{\rm min}$ constraint, where $z_U({\rm UAS}) = \min\{z_{\rm thin}, z_E({\rm UAS})\}$ implements the $d_{\rm max}$ constraint with $z_E({\rm UAS})$ given by Eq. (47), and where $z_L({\rm UAS}) = z_B({\rm UAS})$ implements the $d_{\rm min}$ constraint with $z_B({\rm UAS})$ given in Eq. (43).

Alternatively, one can solve the constraints of the first approach explicitly for the $(z_{\rm dk}, \theta_n)$-integration boundaries. As with the HAS events, the results again bifurcate, depending on whether $z_E({\rm UAS}) < z_{\rm thin}$ (the shower extinguishes), or $z_E({\rm UAS}) > z_{\rm thin}$ (the shower runs out of air). For the case where the shower extinguishes, the boundaries are given by $z_{\rm dk} < \hat{z}({\rm UAS})$ with the latter quantity defined in Eq. (48), and by Eq. (49). For the case where the shower strikes the ''too-thin'' altitude, the boundaries are given by $z_{\rm dk} > \hat{z}({\rm HAS})$ and by Eq. (50).

D. Four constraints for UAS, including Earth's curvature

So far we have treated z as the vertical height above a flat Earth. As remarked in the section on HAS rates, this is a valid approximation as long as the trajectory in the atmosphere is small relative to the Earth's radius $R_\oplus$. Such is the case with HAS events. However, at 10^{20} eV, the decay MFP for a tau is nearly 5000 km, comparable to $R_\oplus$ (6371 km). At extreme energies, curvature effects cannot be neglected for UAS events. Specifically, the error made in the vertical height, as a function of the atmospheric path length w and angle $\theta_{\rm hor}$, is [neglecting terms of order $\mathcal{O}(w^4/R_\oplus^3)$]:

$$\delta z = \frac{w^2}{2R_\oplus} \frac{\cos^2\theta_{\rm hor}}{1 + \frac{w}{R_\oplus}\sin\theta_{\rm hor}} \le \frac{w^2}{2R_\oplus}. \quad (52)$$

The far RHS expression, $w^2/2R_\oplus = 78(w/10^3\ {\rm km})^2$ km, is saturated for (near) horizontal events. The error δz in the height of the decaying tau can be considerable: ~2000 km for nearly horizontal events with $E_\tau \sim 10^{20}$ eV, and ~20 km for nearly horizontal events with $E_\tau \sim 10^{19}$ eV. So our neglect of Earth's curvature means that we underestimate the height of the shower, and so overestimate the air density for shower development. The height underestimate will erroneously reduce (increase) the event rate as viewed from space (ground) when we introduce clouds. The density overestimate will erroneously enhance shower development.

The curved geometry is shown in Fig. 5. The net effects of curvature are twofold. First, for a given path length w and trajectory angle θ_n at emergence from the Earth, the curvature-corrected altitude, which we label as z', is increased. Second, the angle of the shower with respect to a plane tangent to the Earth directly below, which we label as $\theta'_{\rm hor}$ and θ'_n for the horizontal and nadir angles, respectively, are rotated relative to the comparable emergence angles (again, for a given w and θ_n). Note that the primed variables are the altitude (z') and angle (θ') seen by a detector. The unprimed variables describe the shower's prehistory.

We now list the geometric relations which we need. From applying the Pythagorean theorem to the right triangle in Fig. 5, we get z' in terms of w and $\theta_{\rm hor}$:

$$1 + \frac{z'}{R_\oplus} = \left(1 + \left(\frac{w}{R_\oplus}\right)^2 + 2\left(\frac{w}{R_\oplus}\right)\sin\theta_{\rm hor}\right)^{1/2}. \quad (53)$$

Applying the Law of Sines to the same right triangle, we get

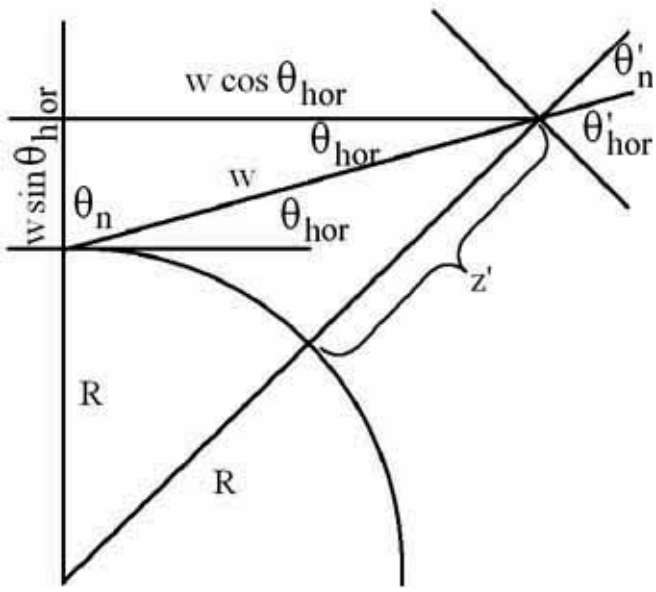

FIG. 5. Illustration of the dependence of shower variables on the Earth's curvature. For clarity, the various parts are not drawn to proportion.

$$\sin\theta'_n = \cos\theta'_{\rm hor} = \frac{\sin\theta_n}{1+\frac{z'}{R_\oplus}} = \frac{\cos\theta_{\rm hor}}{1+\frac{z'}{R_\oplus}}, \tag{54}$$

with $z'(w, \theta_{\rm hor})$ given in Eq. (53). From this comes

$$\cos\theta'_n = \sin\theta'_{\rm hor} = \frac{\sin\theta_{\rm hor}+\frac{w}{R_\oplus}}{1+\frac{z'}{R_\oplus}}, \tag{55}$$

and

$$\cot\theta'_n = \tan\theta'_{\rm hor} = \tan\theta_{\rm hor} + \frac{w}{R_\oplus\cos\theta_{\rm hor}}. \tag{56}$$

This last expression shows clearly that for nearly tangent (''Earth-skimming'') events, the observed angle ($\theta'_{\rm hor}$) is increased from the emergent angle by the term $\approx w/R_\oplus$.

In particular, the altitude and the angle at the decay point of the tau are obtained by setting w equal to $w_{\rm dk}$ in Eqs. (53)–(56). For example, the decay altitude $z'_{\rm dk}$ is given by

$$\frac{z'_{\rm dk}}{R_\oplus} = \left(1+\left(\frac{w_{\rm dk}}{R_\oplus}\right)^2 + 2\left(\frac{w_{\rm dk}}{R_\oplus}\right)\sin\theta_{\rm hor}\right)^{1/2} - 1. \tag{57}$$

After the tau decays, the resulting shower has a length which is short on the scale of $R_\oplus$. Consequently, we may ignore the Earth's curvature from $w_{\rm dk}$ onward, and use $\theta'_{\rm hor}$ and θ'_n as *the* shower angles.

The development of the shower constraints with curvature parallels that for UAS events without curvature, but with (z', θ'_n) rather than (z, θ_n) parametrizing the shower altitude and angle.

The ''too-thin'' shower constraint now becomes

$$z'_{\rm dk}(w_{\rm dk}, \theta_{\rm hor}) \le z_{\rm thin}. \tag{58}$$

Using Eq. (57), this constraint can be cast as a constraint on the integration variables $w_{\rm dk}$ and $\theta_{\rm hor}$ (equivalently, L). The result is

$$w_{\rm dk} \le w^{\rm max}_{\rm dk}(\theta_{\rm hor}, z_{\rm thin}), \tag{59}$$

with

$$\frac{w^{\rm max}_{\rm dk}}{R_\oplus} = \sqrt{\sin^2\theta_{\rm hor} + \left(\frac{z_{\rm thin}}{R_\oplus}\right)\left(2+\frac{z_{\rm thin}}{R_\oplus}\right)} - \sin\theta_{\rm hor}. \tag{60}$$

This constraint requires the decay to occur at an altitude below $z_{\rm thin}$, but does not require a minimum of shower development or a minimum of projected length. The shower development and $l_{\rm min}$ constraints to come will be stronger. However, one useful feature of this constraint is that it defines the maximum decay distance available to a tau in our curved atmosphere. Taking $\theta_{\rm hor} = 0$ to maximize the available decay length, one finds

$$w^{\rm max}_{\rm dk} \le w^{\rm max}_{\rm dk}(\theta_{\rm hor}=0) = \sqrt{z_{\rm thin}(2R_\oplus + z_{\rm thin})}$$
$$\simeq 550\sqrt{\frac{z_{\rm thin}}{3h}}\ {\rm km}. \tag{61}$$

The mean decay length for a tau is already 490 km at 10^{19} eV, and grows linearly with its energy. Thus, it is clear from Eq. (61) that the Earth's curvature significantly reduces the UAS rate at energies at and above 10^{19} eV. It is also clear from (61) that, since $w^{\rm max}_{\rm dk} \ll R_\oplus$, leading order expansions in the ratio $w/R_\oplus$ are valid. For example, to very good approximations, Eqs. (55) and (57) can be written as

$$\sin\theta'_{\rm hor} = \sin\theta_{\rm hor} + \frac{w_{\rm dk}}{R_\oplus}, \tag{62}$$

and

$$z'_{\rm dk} \approx w_{\rm dk}\sin\theta_{\rm hor} + \frac{w^2_{\rm dk}}{2R_\oplus}. \tag{63}$$

The first term on the RHS is just $z_{\rm dk}$ for a ''flat Earth.'' So we learn that the replacement of $z_{\rm dk}$ with $z'_{\rm dk}$ in Eq. (63), like that of $\theta_{\rm hor}$ (at small angle) with $\theta'_{\rm hor}$ in Eq. (56), is a simple translation.

The constraints from shower development require explicit expressions for the shower column density $d(w_{\rm dk}, \theta_n)$ and shower length. The column density in the observer's primed coordinates is

$$d({\rm UAS}; z') = \int_{w_{\rm dk}} dw\rho(z') = \int_{z'_{\rm dk}}^{z'} \frac{dz'}{\cos\theta'_n}\rho(z')$$
$$= \frac{d_{\rm vert}}{\cos\theta'_n}(e^{-z'_{\rm dk}/h} - e^{-z'/h}), \tag{64}$$

with the variables θ'_n and $z'_{\rm dk}$ depending on just $w_{\rm dk}$ and θ_n. Changing $z \to z'$ and $\theta \to \theta'$ in Eqs. (42) and (45) defines $z'_B({\rm UAS})$ and $z'_E({\rm UAS})$, respectively. The explicit expressions for $z'_B({\rm UAS})$ and $z'_E({\rm UAS})$ are given by applying $z \to z'$ and $\theta_n \to \theta'_n$ to Eqs. (43) and (47), respectively. The results are

$$z'_B({\rm UAS}) = -h\ln\left[e^{-z'_{\rm dk}/h} - \frac{d_{\rm min}}{d_{\rm vert}}\cos\theta'_n\right], \tag{65}$$

and

$$z'_E({\rm UAS}) = -h\ln\left[e^{-z'_{\rm dk}/h} - \frac{d_{\rm max}}{d_{\rm vert}}\cos\theta'_n\right]. \tag{66}$$

The $l_{\rm min}$ constraint is

$$[z'_U - z'_L]\tan\theta'_n > l_{\rm min}, \tag{67}$$

with

$$z'_U = \min\{z'_E({\rm UAS}), z_{\rm thin}\}, \qquad \text{and} \quad z'_L = z'_B({\rm UAS}). \tag{68}$$

An algorithm has emerged for including Earth curvature in our prior calculations. We simply replace the unprimed variables $z_{\rm dk}, \theta_n, z_B({\rm UAS}), z_E({\rm UAS})$ with $z'_{\rm dk}, \theta', z'_B({\rm UAS}), z'_E({\rm UAS})$, where $z'_{\rm dk}(z_{\rm dk}, \theta_n)$ and $\theta'_n(z_{\rm dk}, \theta_n)$ are given in Eqs. (53)–(56), and $z'_B({\rm UAS})$ and $z'_E({\rm UAS})$ are given in Eqs. (65) and (66). Note that the parameters $z_{\rm thin}$, $z_{\rm ground}$,

and soon-to-be-introduced $z_{\rm cloud}$ are never primed, for they define layers concentric with the spherical Earth.

At this point we can summarize very easily the UAS constraints including the Earth's curvature (in the absence of cloud cover). We have again the general rate equation, Eq. (4), with inputs from Eqs. (5), (6), (8)–(12), and (23). The ''too-thin'' constraint is given by Eq. (58), or equivalently, by Eqs. (59) and (60). The $l_{\rm min}$ constraint is given by Eqs. (67) and (68), with z'_B(UAS) in Eq. (65) implementing the $d_{\rm min}$ constraint and z'_E(UAS) in Eq. (66) implementing the $d_{\rm max}$ constraint. Unprimed variables are obtained from primed variables via Eqs. (53)–(56), or to a very good approximation via the simplified Eqs. (62) and (63). We have used the latter for our numerical computations.

As in the ''flat Earth'' calculation, more algebra can be done when Eq. (68) is substituted into Eq. (67). The result is Eq. (49) for the $l_{\rm min}$ constraint if z'_U(UAS) $< \hat{z}'$(UAS), and Eq. (50) if z'_U(UAS) $> \hat{z}'$(UAS), where $(z_{\rm dk}, \theta_n) \rightarrow (z'_{\rm dk}, \theta'_n)$ in Eqs. (49) and (50), and $\hat{z}'$(UAS) is defined by priming Eq. (48):

$$\hat{z}\,'({\rm UAS}) \equiv -h \ln\left[\frac{d_{\rm max}}{d_{\rm vert}} \cos\theta'_n + e^{-z_{\rm thin}/h}\right]. \qquad (69)$$

However, when these explicit constraints are expressed in terms of the unprimed variables, no easy separation of $z_{\rm dk}$ and θ_n appears to be possible. Consequently, it seems best to treat the constraints as nonlinear relations in the $(z_{\rm dk}, \theta)$-integration space. This is exactly what we do.

As a check on our work, we have regained the ''flat-Earth'' results for UAS from the curved-Earth formalism, by taking the Earth's radius to be very large in the constraint equations [but keeping $R_\oplus$ physical in Eq. (4) and the $L = 2R_\oplus \cos\theta_n$ relation].

IV. SHOWER RATES WITH CLOUDS

The presence of clouds, their distribution, altitude, and optical depth would obviously affect the observed event rates. Hence, when we consider the effect of a cloud layer on the observable event rate, the resulting constraints become more complicated. In addition, the constraints come to depend on whether the detector is above or below the clouds, i.e., on whether the detector is space based or ground based. We will model the cloud layer in a very simplified way as an infinitely thin layer, but with infinite optical depth and we will assign $z_{\rm cloud}$ to be the height of the relevant cloud boundary. However, we will not take into account how the cloud presence could affect the reconstructed shower geometry and energy [36]. For a space-based detector, the only visible air-showers are those at $z > z_{\rm cloud}$, while for a ground-based detector only showers at $z < z_{\rm cloud}$ can be seen. Let us name the four possible event-detection types, UAS and HAS as seen from space (S) or from the ground (G), as UAS $\otimes$ S, UAS $\otimes$ G, HAS $\otimes$ S, and HAS $\otimes$ G, in obvious notation. Our calculation is partitioned into four parts, corresponding to these four event types. We will see that UAS $\otimes$ G and HAS $\otimes$ S event types are easily calculated with only simple modifications of our prior, cloudless formulas. However, the UAS $\otimes$ S and HAS $\otimes$ G event types require more care, since the observed shower may have its origination above or below the cloud boundary for these cases.

In our simplified model, the actual development of the shower does not depend on the presence or absence of clouds. Thus, the expressions for z_B and z_E, determined by the $d_{\rm min}$ and $d_{\rm max}$ constraints, are unchanged. However, the visible projected length of the shower certainly depends on the presence or absence of clouds. We take this into account.

In this section we do not include the effect of the Earth's curvature. In the next section, Sec. V, we include the Earth's curvature along with clouds in the calculations of the UAS rates. We have seen that Earth curvature does not affect the HAS calculation.

A. UAS in ground-based detectors

Looking upward with a UAS $\otimes$ G detector, the observable atmosphere is bounded from above by the cloud layer. In the absence of clouds, the observable atmosphere was bounded from above by $z_{\rm thin}$. Thus, the prior, cloudless calculation applies to the cloudy atmosphere if we just reset the ''too-thin'' height $z_{\rm thin}$ to the cloud boundary $z_{\rm cloud}$.

One feature of this replacement is that the angular constraint on UAS events, traceable back to Eq. (32), becomes

$$\cos\theta_n \leq \frac{d_{\rm vert}}{d_{\rm min}}(1 - e^{-z_{\rm cloud}/h}) \equiv \cos\theta^*_{\rm G}. \qquad (70)$$

If $z_{\rm cloud} \leq -h \ln[(d_{\rm vert} - d_{\rm min})/d_{\rm vert}]$, then $\cos\theta^*_{\rm G}$ is less than 1, presenting a real constraint on the shower direction. With $d_{\rm min} = 400$ g/cm^2, $\cos\theta^*_{\rm G} \leq 1$ occurs for $z_{\rm cloud} \leq 3.9$ km. Thus, for cloud boundaries below this value, near-vertical showers do not satisfy the $d_{\rm min}$ condition. For example, with a cumulus cloud layer at $z_{\rm cloud} = 2$ km, only shower angles $\theta_n > 55°$ are allowed by the $d_{\rm min}$ constraint. For common extrapolations of the neutrino-nucleon cross-section to very high energies, only ''Earth-skimming'' neutrinos are expected to emerge from the Earth at very high energies. For these ''Earth-skimming'' neutrinos, clouds must be very low to affect the rate.

We rewrite the relevant UAS constraint equations with $z_{\rm thin} \rightarrow z_{\rm cloud}$ to include the cloud boundary. The ''too-thin'' constraint in Eq. (39) becomes

$$0 \leq z_{\rm dk} < z_{\rm cloud}. \qquad (71)$$

The $l_{\rm min}$ constraint Eq. (40) is replaced with

$$[\min\{z_E({\rm UAS}), z_{\rm cloud}\} - z_B({\rm UAS})]\tan\theta_n \geq l_{\rm min}, \qquad (72)$$

with z_E(UAS) and z_B(UAS) as before, given in Eqs. (47)

and (43), respectively. This concludes the implicit calculation of the integration boundaries.

Explicit boundaries are obtained by substituting Eqs. (47) and (43) into (72). The result is that the $l_{\rm min}$ constraint is given by Eq. (49) when $z_{\rm dk} < \hat{z}(\mathrm{UAS} \otimes \mathrm{G})$, and by [derivative from Eq. (50) via $z_{\rm thin} \rightarrow z_{\rm cloud}$]

$$z_{\rm dk} < -h \ln\left[\frac{d_{\rm min}}{d_{\rm vert}} \cos\theta_n + e^{(l_{\rm min}/(\tan\theta_n) - z_{\rm cloud})/h}\right], \quad (73)$$

when $z_{\rm dk} > \hat{z}(\mathrm{UAS} \otimes \mathrm{G})$; the critical altitude $\hat{z}(\mathrm{UAS} \otimes \mathrm{G})$ [derivative from Eq. (48) via $z_{\rm thin} \rightarrow z_{\rm cloud}$] is given by

$$\hat{z}(\mathrm{UAS} \otimes \mathrm{G}) \equiv -h \ln\left[e^{-z_{\rm cloud}/h} + \frac{d_{\rm max}}{d_{\rm vert}} \cos\theta_n\right]. \quad (74)$$

As with the no-clouds case, these $l_{\rm min}$ constraints require a sufficiently large normal angle so that the horizontal projection of the shower is visible. The critical angle is obtained from Eq. (51) with the substitution $z_{\rm thin}$ by $z_{\rm cloud}$. The resulting equation is

$$z_{\rm cloud} = -h \ln\left[\frac{d_{\rm max} - d_{\rm min}}{d_{\rm vert}} \frac{\cos\theta_n^{\rm crit}}{e^{l_{\rm min}/(h \tan\theta_n^{\rm crit})} - 1}\right]. \quad (75)$$

The meaning is that, given a cloud layer at $z_{\rm cloud}$, there are no visible events for $\cos\theta_n > \cos\theta_n^{\rm crit}$. Since $z_{\rm cloud}$ is a monotonically increasing function of $\cos\theta_n^{\rm crit}$, this result may be stated in a different way: there are no visible events at $\cos\theta_n > \cos\theta_n^{\rm crit}$ if there is a cloud layer lower than that of Eq. (75). There are no visible events at all if $\cos\theta_n^{\rm crit} = 0$. From Eq. (75), this occurs for the critical cloud altitude

$$z_{\rm cloud}^{\rm crit} = -h \ln\left[\frac{d_{\rm max} - d_{\rm min}}{d_{\rm vert}} \frac{h}{l_{\rm min}}\right]. \quad (76)$$

Thus, clouds completely obscure the detector if $z_{\rm cloud} < z_{\rm cloud}^{\rm crit}$.

To summarize the formulas giving the UAS ⊗ G events even in the presence of cloud cover, the general rate equation is Eq. (4), with inputs from Eqs. (5), (6), (8)–(12), and (23), the ''too-thin'' constraint is given by Eq. (71), the $l_{\rm min}$ constraint by Eq. (72), with $z_E(\mathrm{UAS})$ and $z_B(\mathrm{UAS})$ unchanged from their cloudless expressions, Eqs. (47) and (43), respectively. Alternatively, explicit $l_{\rm min}$ constraints are available in Eq. (49) for $z_{\rm dk} < \hat{z}(\mathrm{UAS} \otimes \mathrm{G})$, and in (73) for $z_{\rm dk} > \hat{z}(\mathrm{UAS} \otimes \mathrm{G})$, with $\hat{z}(\mathrm{UAS} \otimes \mathrm{G})$ defined in Eq. (74). These twin constraints reflect the two possible outcomes of $\min\{z_E(\mathrm{UAS}), z_{\rm cloud}\}$ in Eq. (72).

B. HAS in space-based detectors

Looking downward with a HAS ⊗ S detector, the visible atmosphere is bounded below by the cloud layer. In the absence of clouds, it is bounded below by $z_{\rm ground}$. Thus, the cloudless calculation applies when $z_{\rm ground}$ is reset to $z_{\rm cloud}$. With this type of substitution in mind, we retained the symbol $z_{\rm ground}$ in our prior cloudless formulas, even though its value was zero there. For example, for the HAS ⊗ S events, the angular constraint of Eq. (32) becomes

$$\cos\theta_z \leq \frac{d_{\rm vert}}{d_{\rm min}}(e^{-z_{\rm cloud}/h} - e^{-z_{\rm thin}/h}) \equiv \cos\theta_{\rm S}^*. \quad (77)$$

This constraint ensures that the shower brightens sufficiently above the clouds to become visible. If $z_{\rm cloud} \geq -h \ln(d_{\rm min}/d_{\rm vert} + e^{-z_{\rm thin}/h})$, then $\cos\theta_{\rm S}^* < 1$, being a real constraint on the shower direction. With $d_{\rm min} = 400\ \mathrm{g/cm^2}$, $\cos\theta_{\rm S}^* \leq 1$ for $z_{\rm cloud} \geq 6.6$ km. Cumulus cloud layers rarely rise to this height, and so there is no angular constraint on HAS ⊗ S resulting from cumulus clouds. However, cirrus clouds populate the high atmosphere, and therefore do constrain the HAS ⊗ S angle θ_z.

We rewrite the other relevant HAS constraint equations with $z_{\rm ground} \rightarrow z_{\rm cloud}$ to include the cloud boundary. The ''too-thin'' constraint becomes

$$z_{\rm cloud} \leq z_{\rm int} \leq z_{\rm thin}. \quad (78)$$

The $l_{\rm min}$ constraint Eq. (27) becomes

$$[z_B(\mathrm{HAS}) - \max\{z_E(\mathrm{HAS}), z_{\rm cloud}\}] \tan\theta_z \geq l_{\rm min}, \quad (79)$$

with $z_B(\mathrm{HAS})$ and $z_E(\mathrm{HAS})$ as before, given in Eqs. (30) and (35). This concludes the implicit calculation of the integration boundaries.

Explicit boundaries are obtained by substituting Eqs. (30) and (35) into (79). The result is that the $l_{\rm min}$ constraint is given by Eq. (37), for $z_{\rm int} > \hat{z}(\mathrm{HAS} \otimes \mathrm{S})$, and by the following [derived from Eq. (38) via $z_{\rm ground} \rightarrow z_{\rm cloud}$] for $z_{\rm int} < \hat{z}(\mathrm{HAS} \otimes \mathrm{S})$:

$$z_{\rm int} > -h \ln\left[e^{-(l_{\rm min}/(\tan\theta_z) + z_{\rm cloud})/h} - \frac{d_{\rm min}}{d_{\rm vert}} \cos\theta_z\right]; \quad (80)$$

the critical altitude $\hat{z}(\mathrm{HAS} \otimes \mathrm{S})$, derivative from Eq. (36) via $z_{\rm ground} \rightarrow z_{\rm cloud}$, is

$$\hat{z}(\mathrm{HAS} \otimes \mathrm{S}) \equiv -h \ln\left[e^{-z_{\rm cloud}/h} - \frac{d_{\rm max}}{d_{\rm vert}} \cos\theta_z\right]. \quad (81)$$

To summarize the formulas giving the HAS ⊗ S events even in the presence of a cloud layer, the general rate equation is Eq. (13), with the area given in Eq. (23), the ''too-thin'' constraint is given by Eq. (78), and the $l_{\rm min}$ constraint by Eq. (79), with $z_B(\mathrm{HAS})$ and $z_E(\mathrm{HAS})$ unchanged from their cloudless expressions. Alternatively, explicit expressions for the $l_{\rm min}$ constraint are available in Eq. (80) for $z_{\rm int} < \hat{z}(\mathrm{HAS} \otimes \mathrm{S})$, and in Eq. (37) for $z_{\rm int} > \hat{z}(\mathrm{HAS} \otimes \mathrm{S})$, with $\hat{z}(\mathrm{HAS} \otimes \mathrm{S})$ defined in Eq. (81). These twin constraints reflect the two possible outcomes of $\max\{z_E(\mathrm{HAS}), z_{\rm cloud}\}$ in Eq. (79).

C. UAS in space-based detectors

Looking downward with a UAS ⊗ S detector, the visible atmosphere is bounded below by the cloud layer, but the visible UAS may have begun its development above or below the clouds. Thus, the ''too-thin'' constraint remains

Eq. (39) as in the cloudless calculation. The new $l_{\rm min}$ constraint is

$$[\min\{z_E(\mathrm{UAS}), z_{\rm thin}\} - \max\{z_B(\mathrm{UAS}), z_{\rm cloud}\}]\tan\theta_n \geq l_{\rm min} \tag{82}$$

with z_E(UAS) and z_B(UAS) as before, given in Eqs. (47) and (43), respectively. This concludes the implicit calculation of the integration boundaries. The left-hand side of Eq. (82) makes it clear that generation of a visible UAS requires $z_E(\mathrm{UAS}) > z_{\rm cloud}$ and $z_B(\mathrm{UAS}) < z_{\rm thin}$, and that the clouds are irrelevant when $z_B(\mathrm{UAS}) > z_{\rm cloud}$.

Explicit boundaries, if desired, are obtained by substituting Eqs. (47) and (43) into (82). There are $4! = 24$ *a priori* orderings of the four parameters in the $l_{\rm min}$ constraint. However, the orderings $z_E(\mathrm{UAS}) > z_B(\mathrm{UAS})$ and $z_{\rm thin} > z_{\rm cloud}$ are fixed. This leaves $4!/(2 \times 2) = 6$ possible orderings of the parameters. Of these six orderings, one has $z_B(\mathrm{UAS}) > z_{\rm thin}$ and another has $z_E(\mathrm{UAS}) < z_{\rm cloud}$. These orderings do not produce an observable shower, the former showering too late and the latter showering too early. We are left with four relevant orderings:

(a) $z_{\rm thin} > z_E > z_B > z_{\rm cloud}$;
(b) $z_E > z_{\rm thin} > z_B > z_{\rm cloud}$;
(c) $z_{\rm thin} > z_E > z_{\rm cloud} > z_B$;
(d) $z_E > z_{\rm thin} > z_{\rm cloud} > z_B$.

The first two, (a) and (b), are characterized by $z_B > z_{\rm cloud}$, which restricts $z_{\rm dk}$ according to

$$z_{\rm dk} > -h \ln\left[e^{-z_{\rm cloud}/h} + \frac{d_{\rm min}}{d_{\rm vert}} \cos\theta_n \right]. \tag{83}$$

Ordering (a) characterizes the shower that extinguishes [i.e. $z_{\rm dk} < \hat{z}(\mathrm{UAS})$], while (b) characterizes the shower that reaches the ''too-thin'' air boundary [i.e. $z_{\rm dk} > \hat{z}(\mathrm{UAS})$]. For the two orderings (a) and (b), the clouds do not obscure any part of the visible shower, and the $l_{\rm min}$ formulas of the cloudless section, Sec. III C, apply. The next two orderings, (c) and (d), are characterized by $z_{\rm cloud} > z_B$. For these two orderings, the clouds do obscure part of the visible shower.

However, it may be that, for low values of $z_{\rm cloud}$, there are no events satisfying the topologies specified in (c) and (d) *regardless of whether the cloud layer is actually present at* $z_{\rm cloud}$. For example, with our canonical value $z_{\rm thin} = 3h$, the conditions in (d) require that the shower remain visible over a vertical length at least as long as $(3h - z_{\rm cloud})$. For a small value of $z_{\rm cloud}$, such a shower might never happen, as UAS showers might not both begin below $z_{\rm cloud}$ and survive beyond $3h$. Thus, in order to see if there is some critical altitude below which real clouds would not suppress the rates in UAS $\otimes$ S detectors, we seek the conditions for which categories (c) and (d) do not contribute events *even in the absence of clouds*. Under such conditions, the acceptance for UAS $\otimes$ S is just that of the cloudless case.

For ordering (d), i.e. $z_E(\mathrm{UAS}) > z_{\rm thin}$ and $z_{\rm cloud} > z_B(\mathrm{UAS})$, the $l_{\rm min}$ constraint presents a restriction on θ_n alone,

$$\begin{aligned} &[z_{\rm thin} - z_{\rm cloud}]\tan\theta_n \geq l_{\rm min}, \\ &\qquad \text{or} \quad z_{\rm cloud} \leq z_{\rm thin} - l_{\rm min}/\tan\theta_n. \end{aligned} \tag{84}$$

For ordering (c), i.e., $z_{\rm thin} > z_E(\mathrm{UAS})$ and $z_{\rm cloud} > z_B(\mathrm{UAS})$, the $l_{\rm min}$ constraint is

$$[z_E(\mathrm{UAS}) - z_{\rm cloud}]\tan\theta_n \geq l_{\rm min}. \tag{85}$$

Inputting z_E(UAS) from Eq. (47) leads to a restatement of this latter constraint as

$$z_{\rm dk} > -h \ln\left[\frac{d_{\rm max}}{d_{\rm vert}} \cos\theta_n + e^{-(l_{\rm min}/(\tan\theta_n) + z_{\rm cloud})/h} \right]. \tag{86}$$

Hence, the altitude on the RHS expresses the minimum altitude above which tau decays contribute events to category (c). Since we have argued that the minimum altitude for shower development in category (d) is higher than in (c), the RHS also expresses the minimum altitude above which tau decays contribute events to categories (c) and (d). Thus, the RHS is the minimum altitude above which tau decays produce showers partially obscured by clouds.

This constraint on $z_{\rm dk}$ is analogous to the one in Eq. (49) which sets the minimum value for $z_{\rm dk}$ in the absence of clouds. Since clouds must be more restrictive than no clouds, the RHS of Eq. (86) must be larger than $z_<$ [RHS of Eq. (49)] if categories (c) and (d) are to have events. This happens if

$$z_{\rm cloud} > -h \ln\left[\frac{d_{\rm max} - d_{\rm min}}{d_{\rm vert}} \frac{\cos\theta_n e^{l_{\rm min}/(h\tan\theta_n)}}{e^{l_{\rm min}/(h\tan\theta_n)} - 1} \right]. \tag{87}$$

This is a necessary condition for events to fall into categories (c) and (d). Consequently, the inequality of opposite sign is the *sufficient* condition for clouds to *not* obscure the showers. The RHS of Eq. (87) is a critical cloud altitude.

For the typical parameter choices which we consider, the RHS of Eq. (87), when positive, has a very weak dependence on $\cos\theta_n$. In particular, it does not differ much from its value evaluated at $\cos\theta_n = 0$, which is

$$z_{\rm cloud}^{\rm crit} = -h \ln\left[\frac{d_{\rm max} - d_{\rm min}}{d_{\rm vert}} \frac{h}{l_{\rm min}} \right]. \tag{88}$$

Thus, we may use Eq. (88) as a very good approximation to the RHS of (87). The approximation becomes even better as the cross-section becomes larger, for then UAS events come from more horizontal neutrino trajectories. Conveniently, the definition of $z_{\rm cloud}^{\rm crit}$ in Eq. (88) is identical to that in Eq. (76). Thus, for all practical purposes we can use the same $z_{\rm cloud}^{\rm crit}$ as the critical altitude for space-based and ground-based UAS detectors.[9] Thus we have the complementary situation that clouds below $z_{\rm cloud}^{\rm crit}$ completely obscure UAS $\otimes$ G, but do not affect UAS $\otimes$ S at all. Of

[9]We have checked numerically the accuracy of this statement.

course, clouds above $z_{\rm cloud}^{\rm crit}$ will partially obscure both UAS ⊗ G and UAS ⊗ S. We explore this complementarity in Sec. IV E.

This concludes the explicit construction of the UAS ⊗ S constraints for all four allowed orderings of the parameters. The final event rate is the sum of the contributions from the four allowed orderings. As a check, we note that in the limit $z_{\rm cloud} \to 0$, orderings (c) and (d) no longer contribute, since $z_B > 0$. Thus, we are left with just the two orderings (a) and (b) of the cloudless limit.

To summarize the formulas giving the UAS ⊗ S events even in the presence of a cloud layer, the general rate equation is Eq. (4), with inputs from Eqs. (5), (6), (8)–(12), and (23). The ''too-thin'' constraint is given by (39), the $l_{\rm min}$ constraint by Eq. (82), with z_E(UAS) and z_B(UAS) unchanged from their cloudless expressions (47) and (43). Explicit solutions for the $l_{\rm min}$ constraint, if desired, are given above for the four allowed orderings of the parameters $\{z_E, z_{\rm thin}, z_B, z_{\rm cloud}\}$. The total event rate is the sum of the four contributions.

D. HAS in ground-based detectors

Looking upward with a HAS ⊗ G detector, the visible atmosphere is bounded above by the cloud layer, but the visible HAS may have begun its development above or below the clouds. Thus, the ''too-thin'' constraint remains Eq. (26) as in the cloudless calculation. The $l_{\rm min}$ constraint is

$$[\min\{z_B({\rm HAS}), z_{\rm cloud}\} - \max\{z_E({\rm HAS}), 0\}]\tan\theta_z \geq l_{\rm min} \tag{89}$$

with z_B(HAS) and z_E(HAS) as before, given in Eqs. (30) and (35), respectively. This concludes the implicit calculation of the integration boundaries. Note that the left-hand side of Eq. (89) makes it clear that generation of a visible shower requires $z_E({\rm HAS}) < z_{\rm cloud}$, and that the clouds are irrelevant when $z_B({\rm HAS}) < z_{\rm cloud}$.

As was the case with UAS ⊗ S events, there are four orderings that contribute to the HAS ⊗ G events:

(a) $z_{\rm cloud} > z_B > z_E > 0$;
(b) $z_{\rm cloud} > z_B > 0 > z_E$;
(c) $z_B > z_{\rm cloud} > 0 > z_E$;
(d) $z_B > z_{\rm cloud} > z_E > 0$.

The first two, (a) and (b), are characterized by $z_{\rm cloud} > z_B$. For these two, the clouds do not obscure any part of the visible shower, and the $l_{\rm min}$ formulas of the cloudless section, Sec. III B, apply [ordering (a) characterizes the shower that extinguishes, while (b) characterizes the shower that reaches the ground]. The next two orderings, (c) and (d), are characterized by $z_B > z_{\rm cloud}$. Here, the clouds do obscure part of the visible shower. For ordering (c), i.e., $z_B({\rm HAS}) > z_{\rm cloud}$ and $0 > z_E({\rm HAS})$, the $l_{\rm min}$ constraint presents a restriction on θ_n alone. It is

$$z_{\rm cloud}\tan\theta_z \geq l_{\rm min}. \tag{90}$$

For ordering (d), i.e. $z_B({\rm HAS}) > z_{\rm cloud}$ and $z_E({\rm HAS}) > 0$,

$$[z_{\rm cloud} - z_E({\rm HAS})]\tan\theta_z \geq l_{\rm min}. \tag{91}$$

A short calculation leads to a restatement of this latter constraint as

$$z_{\rm int} < -h\ln\left[e^{(l_{\rm min}/(\tan\theta_z) - z_{\rm cloud})/h} - \frac{d_{\rm max}}{d_{\rm vert}}\cos\theta_z\right]. \tag{92}$$

This concludes the explicit construction of the constraints for all four allowed orderings of the parameters. The final event rate is the sum of the contributions from the four allowed orderings. As a check, we note that, in the limit $z_{\rm cloud} \to z_{\rm thin}$, orderings (c) and (d) no longer contribute, since $z_B < z_{\rm thin}$. Thus, we are left with just the two orderings (a) and (b) of the cloudless limit.

To summarize the formulas giving the HAS ⊗ G events even with a cloud layer present, the general rate equation is Eq. (13), with the area given in Eq. (23). The ''too-thin'' constraint is given by Eq. (26), the $l_{\rm min}$ constraint by Eq. (89), with z_E(HAS) and z_B(HAS) unchanged from their cloudless expressions, Eqs. (35) and (30). Explicit solutions for the $l_{\rm min}$ constraint, if desired, are given above for the four allowed orderings of the parameters z_B(HAS), $z_{\rm cloud}$, z_E(HAS), and $z_{\rm ground} = 0$. The total event rate is the sum of the four contributions.

E. Remark on UAS with clouds

The RHS of Eq. (76) gives the critical altitude below which clouds would completely obscure ground-based UAS detection. The RHS of Eq. (88) gives the critical altitude below which clouds would not affect space-based UAS detection.[10] These two equations are inverse to each other in meaning, but numerically the critical altitudes on the RHS's in these two equations are identical: .

$$z_{\rm cloud}^{\rm crit}({\rm UAS}) \equiv -h\ln\left[\frac{d_{\rm max} - d_{\rm min}}{l_{\rm min}}\frac{h}{d_{\rm vert}}\right]. \tag{93}$$

Here we have factored the argument of the logarithm into a ratio $(d_{\rm max} - d_{\rm min})/l_{\rm min}$ which is determined by the experimental triggers (i.e., by humans and their optics), and the ratio $h/d_{\rm vert} = 1/\rho(0)$, which is Nature's gift of our atmospheric density at sea level [cf. Eq. (15)]. Numerically, the latter term is 8 km/1030 g cm^{-2} = (129 g cm^{-2}/km)$^{-1}$. When the argument of the logarithm is <1, this equation has a positive solution, and so sufficiently low-lying clouds will completely obscure UAS ⊗ G, but not affect at all UAS ⊗ S. There will always be a positive solution $z_{\rm cloud}$ whenever $(d_{\rm max} - d_{\rm min})/l_{\rm min}$ is less than $d_{\rm vert}/h = \rho(0) =$ 129 g cm^{-2}/km.

The range of a visible shower at or near 10^{20} eV is comparable to $d_{\rm vert}$, and so $(d_{\rm max} - d_{\rm min})/d_{\rm vert}$ is of order unity. Typically, the visible length required for shower

[10] To be accurate, it is the minimum of the RHS of (87) which gives the critical altitude, as we explained in Sec. IV C.

identification is of order of $h = 8$ km, so $h/l_{\rm min}$ is also of order unity. Thus, the argument of the logarithm is of order unity. Consequently, whether there can be significant cloud obscuration in UAS ⊗ G and no effect in UAS ⊗ S will depend critically on an experiment's choice of shower parameters, $d_{\rm min}$, $d_{\rm max}$, and $l_{\rm min}$. As relevant examples, with the choices $d_{\rm min} = 400(300)$ g/cm^2 and $d_{\rm max} = 1200(1500)$ g/cm^2, for $l_{\rm min} = 10$ km the argument of the log is <1, $z^{\rm crit}_{\rm cloud}$ is 3.8(0.56) km, and so a cloud layer at a lower altitude will completely suppress observation in UAS ⊗ G detectors and have no effect in UAS ⊗ S detectors. In contrast, for $l_{\rm min} = 5$ km the argument of the logarithm exceeds unity, there is no $z_{\rm cloud}$, and so there is partial rate suppression due to clouds at any altitude for both UAS ⊗ G and UAS ⊗ S.

In Fig. 6 we plot $z^{\rm crit}_{\rm cloud}$(UAS) versus the trigger-parameter combination $(d_{\rm max} - d_{\rm min})/l_{\rm min}$, over the range 30–130 km/g cm^{-2}. As foretold, for values above $d_{\rm vert}/h = \rho(0) = 129$ km/g cm^{-2}, the solution to Eq. (93) is negative and partial cloud suppression occurs in both UAS ⊗ G and UAS ⊗ S for any nonzero value of $z_{\rm cloud}$. But for $(d_{\rm max} - d_{\rm min})/l_{\rm min}$ less than 129 km/g cm^{-2}, there is a positive critical altitude delineating total cloud suppression as seen from ground and no cloud suppression as seen from space, from partial suppression of both. We infer from the figure that an experimental trigger $(d_{\rm max} - d_{\rm min})/l_{\rm min}$ exceeding (50, 80, 100) km/g cm^{-2} is required for (i) UAS ⊗ G to avoid complete rate suppression from clouds below (7.6, 3.8, 2.0) km, while suffering partial suppression from clouds above (7.6, 3.8, 2.0) km; (ii) UAS ⊗ S to have partial rate suppression from clouds above (7.6, 3.8, 2.0) km, while suffering no suppression from clouds below (7.6, 3.8, 2.0) km.

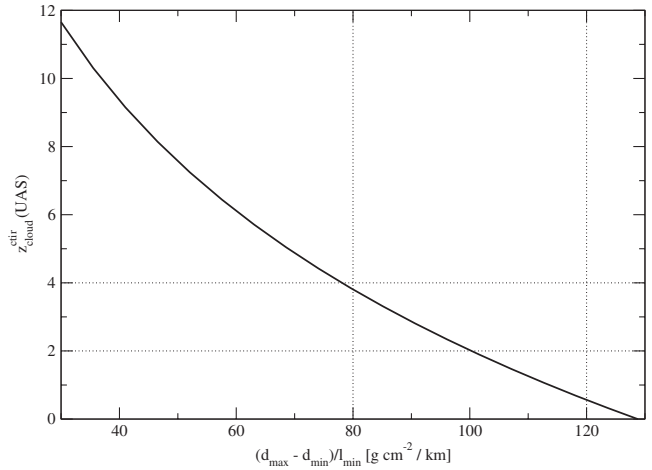

FIG. 6. Critical altitude below which clouds would obscure the detector for UAS ⊗ G and have virtually no effect for UAS ⊗ S. Above the critical altitude, clouds would partially obscure both UAS ⊗ G and UAS ⊗ S. The label on the abscissa can be thought of as an experimental sensitivity to showers. We have taken $d_{\rm vert}/h = 1030$ g cm^{-2}/8 km.

The ground-based result is intuitive, in that as the trigger sensitivity $(d_{\rm max} - d_{\rm min})/l_{\rm min}$ is increased, the experiment may tolerate clouds ever closer to the ground. The space-based result is less intuitive. In this case, as the trigger sensitivity is increased, the critical cloud altitude above which UAS are partially obscured is *again lowered* (after all, the same $z^{\rm crit}_{\rm cloud}$ is common to UAS ⊗ G and UAS ⊗ S). The reason is that, with better triggering, a space-based experiment is sensitive to more effective atmospheric volume, and so to the presence of lower cloud layers. Put another way, with better sensitivity a space-based experiment may see deeper into the atmosphere where the air is denser, but not if there are low-lying clouds.

Notice that we have used our flat-Earth formulas to derive $z_{\rm cloud}$, and the conclusions that follow from it. In particular, we have expressed the condition for cloud suppression of UAS ⊗ G rates and (to very good approximation) cloud nonsuppression of UAS ⊗ S rates analytically without regard to the angles of UAS trajectories. One may ask whether Earth's curvature alters our discussion. Unfortunately, inclusion of curvature leads to transcendental equations, rather than to an improved simple analytic expression. However, from numerical studies we can attest that curvature does not alter our qualitative conclusions. In fact, when only small horizontal-angle UAS events contribute [which holds for most of the cross-section range, cf. Eq. (7)], then our quantitative conclusions are accurate, too.

Finally, we remark that there is no analogue of $z_{\rm cloud}$ for cloud suppression of HAS rates. The HAS constraints are different from the UAS, and HAS trajectories are not restricted to small horizontal angles.

V. UAS WITH CLOUDS AND EARTH CURVATURE

The distance between interaction point and shower extinction for HAS events is sufficiently small that Earth curvature can be neglected. However, we have seen that Earth curvature cannot be neglected for UAS events, since the tau decay path at high energy provides a length large on the scale of the atmospheric height $z_{\rm thin}$. We consider again the two UAS possibilities, viewed from space and viewed from ground. The results of Secs. IV A and IV C for UAS rates with clouds are extended to include also Earth's curvature by priming appropriate variables.

The algorithm for priming was presented in Sec. III D. According to the algorithm, the Earth's curvature is added to our prior "flat-Earth" calculations by simply replacing the unprimed variables $z_{\rm dk}$, θ_n, z_B(UAS), z_E(UAS) with primed variables $z'_{\rm dk}$, θ'_n, z'_B(UAS), z'_E(UAS), where $z'_{\rm dk}(z_{\rm dk}, \theta_n)$ and $\theta'_n(z_{\rm dk}, \theta_n)$ are given in Eqs. (53)–(56), and z'_B(UAS) and z'_E(UAS) are given by priming z_B(UAS), z_E(UAS), $z_{\rm dk}$, θ_n in Eqs. (43) and (47) to get

Eqs. (65) and (66). The parameters $z_{\rm thin}$, $z_{\rm ground}$, $z_{\rm cloud}$ are never primed, for they define layers concentric with the spherical Earth. In what follows, we apply this algorithm explicitly to the ground-based and space-based UAS rates.

A. UAS viewed from ground, with clouds and curvature

Priming the appropriate variables of Sec. IV A, the ''too-thin'' constraint in Eq. (71) becomes

$$0 \leq z'_{\rm dk} < z_{\rm cloud}. \tag{94}$$

The $l_{\rm min}$ constraint Eq. (72) becomes

$$[\min\{z'_E({\rm UAS}), z_{\rm cloud}\} - z'_B({\rm UAS})]\tan\theta'_n \geq l_{\rm min}. \tag{95}$$

This concludes the inclusion of curvature in the integration boundaries of the UAS ⊗ G rate with clouds.

To summarize the formulas giving the UAS ⊗ G events, the general rate equation is Eq. (4), with inputs from Eqs. (5), (6), (8)–(12), and (23), the ''too-thin'' constraint is given by (94), and the $l_{\rm min}$ constraint by Eq. (95), with z'_E(UAS) and z'_B(UAS) given in Eqs. (66) and (65), respectively.

B. UAS viewed from space, with clouds and curvature

Priming appropriately, the ''too-thin'' constraint in Eq. (39) becomes

$$0 \leq z'_{\rm dk} < z_{\rm thin}, \tag{96}$$

and the $l_{\rm min}$ constraint in Eq. (82) becomes

$$[\min\{z'_E({\rm UAS}), z_{\rm thin}\} - \max\{z'_B({\rm UAS}), z_{\rm cloud}\}]\tan\theta'_n \geq l_{\rm min}. \tag{97}$$

This concludes the inclusion of curvature in the integration boundaries of the UAS ⊗ S rate with clouds.

To summarize the formulas giving the UAS ⊗ S events, the general rate equation is Eq. (4), with inputs from Eqs. (5), (6), (8)–(12), and (23). The ''too-thin'' constraint is given by Eq. (96), and the $l_{\rm min}$ constraint by Eq. (97), with z'_E(UAS) and z'_B(UAS) given in Eqs. (66) and (65), respectively.

VI. RESULTS

In this section, we present the results of our semianalytical approach. For ground- and space-based detectors, we show the dependence of the acceptance for HAS and UAS events on neutrino energy, threshold energy, shower length, and shower column density, as a function of the neutrino-nucleon cross-section. For incident neutrino energies, we choose $E_\nu = 10^{20}$ and 10^{21} for illustration, and demonstrate that the ratio of HAS-to-UAS events resulting from these energies would be of great help in determining the neutrino-nucleon cross-section at these very high energies. For the UAS sample, we compute the acceptance for taus emerging over land from pure rock, and separately for taus emerging over the ocean from a water layer overlaying a rock layer; we take the water layer to have a uniform depth of 3.5 km. We also consider the deleterious effects of low or high cloud layers in the atmosphere, as viewed from space and from the ground.

In all figures, we take the FOV and solid angle entering the acceptance calculations to be that of the EUSO design report [35]. This FOV area, entering Eq. (23), is $\pi \times (400/\sqrt{3})^2$ km^2. The solid angle is 2π for either the HAS or the UAS events. The product of area and solid angle is then, very nearly 10^6 km^2 sr.[11] The OWL proposal [37] [two (or more) free-flying satellites] has a larger FOV, and stereo eyes.

Before proceeding with a comparison of the various acceptance curves, it is worthwhile to reflect on what kind of neutrino event rates might arise in very-large EUSO/OWL-scale experiments. The event rate is obtained by simply multiplying the acceptance by Nature's cosmic neutrino flux per appropriate flavor. As discussed in earlier sections, the appropriate flavor for HAS is ν_e (and $\bar{\nu}_e$), since ν_μ and ν_τ interactions ''lose'' 80% of their energy to the escaping charged muon or tau. For UAS, the appropriate flavor is ν_τ, since among the charged leptons only the tau has a radiation length long enough to allow a significant fraction of taus to escape from the Earth. For the UAS case, we weight the ν_τ flux by tau branching fractions and $\tau \rightarrow$ shower energy transfers (2/3 for hadronic showers, 1/3 for electronic showers, and zero for the muonic mode).

The cosmic neutrino flux is a matter for pure speculation at present. A collection of theoretical fluxes is shown in Ref. [38]. We will choose as our benchmark a neutrino flux which is 10 times the integrated flux of cosmic rays at $E_{\rm GZK}$, just below the GZK suppression. Our benchmark (BM) value is

$$\frac{d\mathcal{F}_{\rm BM}}{dA d\Omega dt} \equiv 10 \times \frac{d\mathcal{F}_{\rm CR}(>E_{\rm GZK})}{dA d\Omega dt} = \frac{1}{\rm km^2\,sr\,yr}. \tag{98}$$

The factor of 10 is included to give a simple number for the benchmark flux.

A popular alternative benchmark neutrino flux is that of Waxman and Bahcall (WB) [39], who offered arguments relating the high-energy neutrino flux to the observed high-

[11] A simple estimate of the instantaneous EUSO acceptance for HAS cosmic-ray events is readily obtained by multiplying this $A \times 2\pi$ value by $\frac{1}{2}$ to account for the mean projection of the FOV normal to the source. The result is a naive HAS acceptance of $\sim 5 \times 10^5$ km^2 sr for cosmic rays. For neutrinos, the detection efficiency is less than unity by the factor $\sim 2h\rho(0)\sigma^{\rm CC}_{\nu N}$. The factor of 2 arises because the mean path length in the atmosphere of a neutrino is twice the vertical value. Put another way, the increased interaction probability for oblique trajectories compensates the $\frac{1}{2}$ coming from projecting the FOV normal to the mean neutrino direction (cosines cancel). These simple HAS acceptances assume 100% detection efficiencies. Incidentally, the discriminator between cosmic-ray initiated HAS and neutrino initiated HAS is the depth of origin of the shower in the atmosphere.

energy cosmic-ray flux. They obtained

$$\frac{d\mathcal{F}_{\rm WB}}{dAd\Omega dt} = \frac{6\times 10^{-2}(10^{20}\ {\rm eV}/E_\nu)}{{\rm km}^2\ {\rm sr\,yr}}. \qquad (99)$$

Subsequent discussion has shown that their arguments, while sensible, are not compelling. Predictions of the cosmogenic neutrino flux [40], resulting from charged-pion production in the GZK process and subsequent pion decay, gives fluxes of order of the WB benchmark. Proposed sources of a more exotic nature give larger fluxes.

In reality, only Nature knows the value of the real flux. It could be larger than these benchmarks, it could be smaller, or it could even be zero. For our benchmark flux, an acceptance of one km^2-sr is required to yield one event per year. For Nature's flux, the event rate is $\frac{d\mathcal{F}_\nu(E_\nu>E_*)}{dAd\Omega dt}/\frac{d\mathcal{F}_{\rm BM}}{dAd\Omega dt}$, where E_* is the minimum neutrino energy producing observable events in the detector with efficiency of order unity. We use units of (km^2 sr) when we plot acceptances. The fluxes and rates we have just discussed give a real physical meaning to these acceptance units.

In Fig. 7 are plotted UAS (solid and dashed) and HAS (dotted) acceptances in our standard units of (km^2 sr), versus fixed values of $\sigma^{\rm CC}_{\nu N}$, for the ideal case of a cloudless sky. Five separate dependences are illustrated in this figure: UAS vs HAS; $E_\nu = 10^{20}$ eV vs 10^{21} eV; over ocean vs over land; shower-threshold energy $E^{\rm sh}_{\rm th} = 10^{19}$ eV vs 5×10^{19} eV; and minimum shower length $l_{\rm min} = 10$ km vs 5 km. Shower-evolution parameters are set to $d_{\rm min} = 400$ g/cm^2 and $d_{\rm max} = 1200$ g/cm^2. A sixth possible dependence is whether the shower is viewed from above by a space-based observatory, or from the below by a ground-based observatory. Within the approximations of this paper, there is no difference between the acceptances for ground-based and space-based detectors *in the cloudless case*. However, there are significant up-down differences when the sky includes clouds.

The HAS acceptances depend on neutrino energy only via $\sigma^{\rm CC}_{\nu N}(E_\nu)$, and rise linearly with $\sigma^{\rm CC}_{\nu N}$. Plotted against $\sigma^{\rm CC}_{\nu N}$, then, the straight-line HAS curves (dotted) are universal curves valid for any E_ν exceeding the trigger threshold $E^{\rm sh}_{\rm th}$. The UAS acceptances have a complicated dependence on E_ν; it arises from the energy dependences of ν propagation in the Earth, tau propagation in the Earth, and path length of the tau in the atmosphere before it decays, the latter also affecting the visible-shower characteristics. In each panel, we show UAS acceptances for two different incident neutrino energies, 10^{21} eV (thick lines) and 10^{20} eV (thin lines). The solid lines show the UAS acceptances for trajectories emerging from the ocean, and dashed lines show the UAS acceptances for trajectories emerging from land, having traveled through only rock.

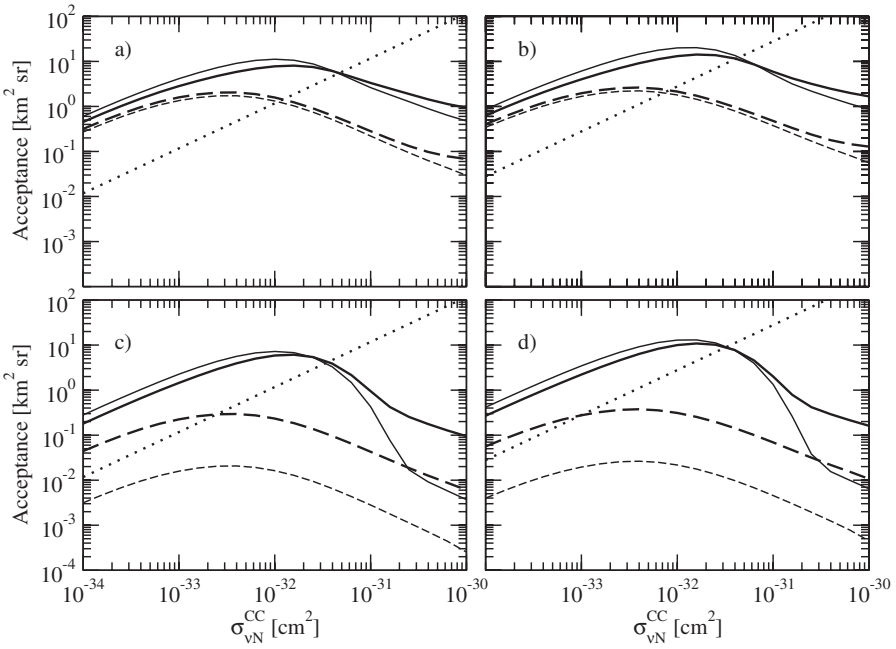

FIG. 7. Acceptances for space-based (or ground-based) detectors in the absence of clouds. Values of $d_{\rm min}$ and $d_{\rm max}$ are fixed at 400 and 1200 g/cm^2, respectively. The curves correspond to HAS (dotted line), which are independent of E_ν except through $\sigma^{\rm CC}_{\nu N}(E_\nu)$; and UAS over ocean with $E_\nu = 10^{21}$ eV (thick solid line), ocean with $E_\nu = 10^{20}$ eV (thin solid line), land with $E_\nu = 10^{21}$ eV (thick dashed line), and land with $E_\nu = 10^{20}$ eV (thin dashed line). Panels are for (a) $E^{\rm sh}_{\rm th} = 10^{19}$ eV and $l_{\rm min} = 10$ km; (b) $E^{\rm sh}_{\rm th} = 10^{19}$ eV and $l_{\rm min} = 5$ km; (c) $E^{\rm sh}_{\rm th} = 5\times 10^{19}$ eV and $l_{\rm min} = 10$ km; (d) $E^{\rm sh}_{\rm th} = 5\times 10^{19}$ eV and $l_{\rm min} = 5$ km. For reference, a popular QCD extrapolation of the neutrino-nucleon cross-section [11] gives 0.54 and 1.2 times 10^{-31} cm^2 at $E_\nu = 10^{20}$ and 10^{21} eV, respectively; the known CC cross-section is 2×10^{-34} cm^2 at an equivalent energy on fixed-target of 5×10^{13} eV, the highest energy for which measurement has been made (at HERA).

For trajectories emerging from the ocean, the taus typically travel through rock and water.

Two different shower-threshold energies are shown, $E_{\rm th}^{\rm sh} = 10^{19}$ eV in the upper two panels and $E_{\rm th}^{\rm sh} = 5 \times 10^{19}$ eV in the lower two panels. The EUSO experiment is working to lower its threshold trigger from $E_{\rm th}^{\rm sh} = 5 \times 10^{19}$ eV to 10^{19} eV, in order to better overlap events from the Auger experiment (the Auger threshold is $\sim 10^{18}$ eV). Also explored in the different panels of Fig. 7 is the dependence of the acceptance on the minimum shower length required for experimental identification. In the two left panels we have taken $l_{\rm min} = 10$ km, while in the two right panels we took $l_{\rm min}$ equal to half of that, 5 km.

Several trends are evident in Fig. 7. We can clearly see that the UAS acceptance (and so also the rate) is typically an order of magnitude larger when neutrinos traverse a layer of ocean water, compared to a trajectory where they only cross rock. Thus, the UAS event rate is enhanced over the ocean relative to over land [41]. The value of this enhancement depends on the shower threshold energy $E_{\rm th}^{\rm sh}$ of the detector (upper versus lower panels) and on the neutrino-nucleon cross-section (the abscissa) in a nontrivial way. One sees general trends that (i) the larger the cross-section and threshold energy are, the larger is the relative enhancement; (ii) the lower the threshold energy is, the closer are the acceptances for different initial neutrino energies (thick vs thin lines); and for high $E_{\rm th}^{\rm sh}$ approaching E_ν, there is a significant suppression of events over land, and over water for larger cross-sections. Lower threshold energies are of course also advantageous in that they necessarily imply larger total event rates.

The sensitivity to $E_{\rm th}^{\rm sh}$ is partly due to the various energy transfers from the tau to the shower in the different tau-decay modes. We have remarked that for the hadronic/electronic/muonic decay modes, $\frac{2}{3}/\frac{1}{3}/0$ of the tau energy goes into the shower. This means that a neutrino with an incident energy of 10^{20} eV characteristically produces a tau with energy 0.8×10^{20} eV, which then produces hadronic/electronic showers with mean energies *at most* (after allowing for the tau's dE/dx in the Earth) $5.3/2.7 \times 10^{19}$ eV. Clearly, the electronic mode is below the $E_{\rm th}^{\rm sh} = 5 \times 10^{19}$ eV threshold, and the hadronic mode is barely above. Both modes are above the $E_{\rm th}^{\rm sh} = 10^{19}$ eV threshold.

We obtain benchmark event rates by multiplying our calculated acceptances with the benchmark integrated flux, Eq. (98), of one neutrino per (km^2 sr yr). The result is a signal exceeding an event per year for an acceptance exceeding a (km^2 sr). Thus we see that the benchmark flux gives a HAS rate exceeding 1/yr if $\sigma_{\nu N}^{\rm CC}$ exceeds 10^{-32} cm^2; and an UAS rate exceeding 1/yr over water for the whole cross-section range with $E_{\rm th}^{\rm sh} = 10^{19}$ eV, and over land if $\sigma_{\nu N}^{\rm CC} \lesssim 10^{-31}$ cm^2. When $E_{\rm th}^{\rm sh}$ is raised to 5×10^{19} eV, however, the UAS signal over land is seriously compromised, while UAS rates over the ocean are little changed. HAS rates are unchanged, as long as E_ν exceeds $E_{\rm th}^{\rm sh}$.

It is interesting that in the UAS case over the ocean, the acceptances at $E_\nu = 10^{20}$ and 10^{21} eV as a function of $\sigma_{\nu N}^{\rm CC}$ are seen to cross. For lower values of the cross-section, the acceptance is larger when the initial neutrino energy is smaller, unlike what might naively be expected. This is due to the combined effect of larger nadir angles θ_n contributing at lower neutrino energy, the nature of energy losses in water vs rock, and the trigger constraints imposed on the showers. For larger cross-sections, only small-angle Earth-skimming neutrinos contribute, so the propagation of the tau lepton happens mostly in water; complications are mainly absent and hence larger initial neutrino energies give larger acceptances, in agreement with intuition.

We call attention to the fact that, for UAS over both ocean and land, there is a maximum in the UAS acceptance at cross-section values $\sigma_{\nu N}^{\rm CC} \sim (1\text{–}2) \times 10^{-32}$ cm^2 and $\sigma_{\nu N}^{\rm CC} \sim (0.3\text{–}0.5) \times 10^{-32}$ cm^2, respectively. For cross-sections similar or smaller than those at the maximum, the acceptance for UAS is larger than that for HAS; conversely, for cross-sections above those at the maximum, HAS events will dominate UAS events. The cross-section value at the maximum lies just below the extrapolation of the standard model cross-section, which for the two initial neutrino energies considered, 10^{20} eV and 10^{21} eV, is 0.54×10^{-31} cm^2 and 1.2×10^{-31} cm^2, respectively. If this extrapolation is valid, then one would expect comparable acceptances (and event rates) for UAS over water and for HAS; the acceptance for UAS over land is down from these by an order of magnitude. If the true cross-section exceeds the extrapolation, then HAS events will dominate UAS events; if the true cross-section is suppressed compared to the extrapolation, then UAS events will dominate HAS events. Importantly, the very different dependences on the cross-section of the HAS (linear) and UAS acceptances offers a practical method to measure $\sigma_{\nu N}^{\rm CC}$. One has simply to exploit the ratio of UAS-to-HAS event rates.

Furthermore, the shape of the UAS acceptance with respect to $\sigma_{\nu N}^{\rm CC}$ establishes the ''cannot lose theorem'' [21], which states that, although a large cross-section is desirable to enhance the HAS rate, a smaller cross-section still provides a robust event sample due to the contribution of UAS. The latter sample is especially abundant over the ocean.

Finally, from the comparison of left ($l_{\rm min} = 10$ km) and right ($l_{\rm min} = 5$ km) panels, one infers the sensitivity of acceptance to the experimental trigger for visible-shower length. We see that reducing the minimum shower length by a factor of 2 here increases the acceptance by roughly a factor of 3 for HAS, and slightly less for UAS. So for a cloudless sky, not too much is lost by choosing longer showers for event reconstruction. This is fortunate, for, as remarked early in Sec. III, the signal/noise and angular reconstruction are greater for longer showers. We forewarn that the sensitivity to the $l_{\rm min}$ trigger will become extreme when we consider a sky with clouds, which we address next.

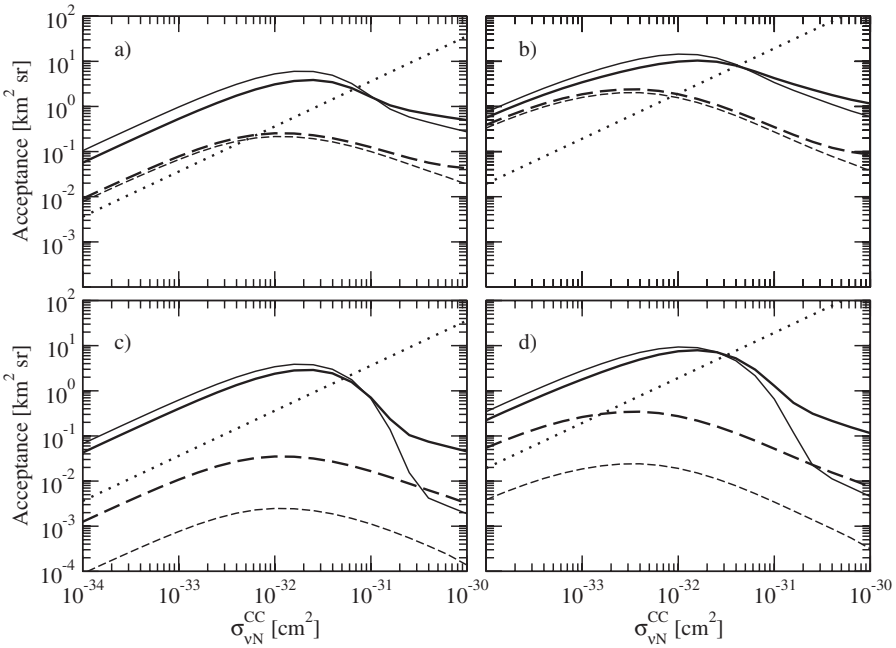

FIG. 8. Acceptances in the presence of a cloud layer at $z_{\rm cloud} = 2$ km; with $l_{\rm min}$ fixed at 5 km, $d_{\rm min}$ at 400 g/cm^2, and $d_{\rm max}$ at 1200 g/cm^2. The curves correspond to HAS (dotted line), which are independent of E_ν except through $\sigma^{\rm CC}_{\nu N}(E_\nu)$; and UAS over ocean with $E_\nu = 10^{21}$ eV (thick solid line), ocean with $E_\nu = 10^{20}$ eV (thin solid line), land with $E_\nu = 10^{21}$ eV (thick dashed line), and land with $E_\nu = 10^{20}$ eV (thin dashed line). Panels are for (a) ground-based detectors with $E^{\rm sh}_{\rm th} = 10^{19}$ eV; (b) spaced-based detectors with $E^{\rm sh}_{\rm th} = 10^{19}$ eV; (c) ground-based detectors with $E^{\rm sh}_{\rm th} = 5 \times 10^{19}$ eV; (d) spaced-based detectors with $E^{\rm sh}_{\rm th} = 5 \times 10^{19}$ eV.

In Fig. 8 are shown the acceptances in the presence of a cumulus cloud layer at 2 km, again as a function of $\sigma^{\rm CC}_{\nu N}$, and again with $d_{\rm min} = 400$ g/cm^2 and $d_{\rm max} = 1200$ g/cm^2. We model the cloud layer as infinitely thin with altitude $z_{\rm cloud}$, but with an infinite optical depth so that showers are completely hidden on the far side of the cloud layer. Details of this modeling were given in Secs. IV and V. We call low-lying cloud layers ''cumulus,'' and high-lying layers ''cirrus,'' for obvious reasons.

For a sky with clouds, we show acceptances for $l_{\rm min}$ set to 5 km. We do not show the case with $l_{\rm min} = 10$ km, because with low-lying clouds, the UAS acceptances for ground-based detectors are essentially zero with $l_{\rm min} = 10$ km (and $d_{\rm min} = 400$ g/cm^2 and $d_{\rm max} = 1200$ g/cm^2). On the other hand, the space-based rates are virtually unaffected by the low clouds. For the UAS as seen from the ground, there simply is not enough space below the cloud layer for the Earth-skimming tau to decay and for the subsequent shower to develop [see Eqs. (75) and (87)]. The smaller $l_{\rm min} = 5$ km that we do show allows enough UAS events to develop into an observable shower below the cloud layer to establish a meaningful acceptance for ground-based detectors. Recall, however, that the UAS rate suppression due to clouds depends sensitively on the value of $(d_{\rm max} - d_{\rm min})/l_{\rm min}$. If the value of this is larger than $d_{\rm vert}/h$, the suppression is aggravated for space-based UAS and alleviated for ground-based UAS, and vice versa [as discussed below Eqs. (75) and (87), and more extensively in Sec. IV E].

Since we show one value of $l_{\rm min}$, not two, in Fig. 8, the number of panels is half that in Fig. 7. On the other hand, the symmetry between upward-looking ground-based detectors, and downward-looking space-based detectors is broken by the cloud layer, so we must now show separate panels for the space-based and ground-based detectors. This brings the number of panels back to four. The HAS and UAS curves are represented in the same way in Fig. 8 as for Fig. 7. The thick and thin lines bear the same meanings for the initial neutrino energies. The left panels show acceptances for ground-based detectors, whereas the right panels show those of space-based detectors. As with the previous figure, the upper panels show results for a threshold energy of $E^{\rm sh}_{\rm th} = 10^{19}$ eV, and the lower panels for $E^{\rm sh}_{\rm th} = 5 \times 10^{19}$ eV.

We see from this figure that qualitative features learned for the cloudless case apply also in this cloudy case. One difference is that the UAS acceptances over land in panel (c) are smaller than the HAS acceptance over the entire range of $\sigma^{\rm CC}_{\nu N}$. One may judge the effect of clouds by comparing Fig. 8 against the $l_{\rm min} = 5$ km panels (b) and (d) of the clear-sky Fig. 7. Quantitatively, the ground-based acceptances (left panels in Fig. 7) are quite reduced by the low-lying clouds, whereas the space-based acceptances (right panels) are not, as one would expect. The suppression of the ground-based acceptance is most severe for small cross-sections, for which the tau leptons emerge more vertically and disappear into the clouds before their eventual shower occurs and develops. Ground-based UAS

acceptances are reduced by up to an order of magnitude over water, and even more over land. Ground-based HAS acceptances, still linear in $\sigma_{\nu N}^{\mathrm{CC}}$, are reduced by an order of magnitude. For space-based detectors, the UAS acceptance is reduced little by clouds at 2 km. Larger neutrino cross-sections lead to more tangential tau showers which may hide below a low-lying cloud layer. We see that UAS reductions are a factor of 2 for the larger cross-sections shown, and less for the smaller values of cross-section.

The dramatic reduction of ground-based acceptances by low-lying cumulus clouds begs the question, ''what are the effects of higher-altitude clouds on space-based detectors?'' In Fig. 9, we continue the study of the dependence of space-based acceptances on cloud altitude. We also examine the suppressing effect of the Earth's curvature.

Fixed values in Fig. 9 are $l_{\mathrm{min}} = 5$ km, and threshold energies of $E_{\mathrm{th}}^{\mathrm{sh}} = 10^{19}$ eV in the left panel and 5×10^{19} eV in the right panel. All curves representing UAS assume events over water and an initial neutrino energy of 10^{20} eV; curves for HAS are valid for any energy exceeding $E_{\mathrm{th}}^{\mathrm{sh}}$. Acceptances for two cloud altitudes, $z_{\mathrm{cloud}} = 4$ km (thick curves) and 12 km (thin curves), are shown for HAS (solid curves) and UAS (dashed curves). Results are to be compared with the thin solid (UAS) and thin dotted (HAS) lines in panels (b) and (d) of Figs. 7 and 8. We infer from comparing these three figures that the effect on a space-based detector of higher cumulus clouds, and even higher cirrus clouds, is more dramatic for downgoing HAS $\otimes$ S than for upcoming UAS $\otimes$ S. The HAS acceptance is reduced by factors of $\sim$1.5, 3, and 10 when the cloud layer lies at $z_{\mathrm{cloud}} = 2$, 4, and 12 km, respectively. In contrast, the UAS acceptance is reduced by factors of $\sim$1.5, 2, and 3 when the cloud layer lies at $z_{\mathrm{cloud}} = 2$, 4, and 12 km, respectively. Since cloud layers are common, they will compromise the acceptance of space-based detectors.

Also shown in both panels of Fig. 9 are the UAS acceptances (dotted lines) for a flat Earth. One sees that correct inclusion of the Earth's curvature lowers the acceptance, since it puts the tau decay and the subsequent onset of shower evolution into the thinner air of higher altitudes. Curvature does little harm for smaller cross-sections, but reduces the acceptance for $\sigma_{\nu N}^{\mathrm{CC}} \gtrsim 0.5 \times 10^{-31}$ cm^2. Coincidentally, 0.5×10^{-31} cm^2 is the popular value for the QCD-extrapolated cross-section. The reduction of acceptance for larger cross-sections is understandable, because the for larger $\sigma_{\nu N}^{\mathrm{CC}}$ the taus emerge from the Earth more horizontally, and hence travel more lateral distance before they decay. The Earth ''falls away'' from the taus as $(\text{lateral displacement})^2/2R_{\oplus}$. Beyond $\sim 10^{-31}$ cm^2, the reduction factor is about 2.5 for cloud layers at either 4 or 12 km (and quite different for E_{ν} near $E_{\mathrm{th}}^{\mathrm{sh}}$).

Since curvature raises the altitude of the tau shower [and rotates it toward the vertical by $\theta \sim (\text{lateral displacement})/R_{\oplus}$)], the net effect is to remove the bottom layer of atmosphere from the UAS shower development. Clouds remove the bottom layer from view for UAS $\otimes$ S. Thus, one expects the reduction in acceptance due to Earth's curvature to be largest in the cloudless case. We have checked numerically that for the parameters of Fig. 8, a reduction factor of $\sim$3.5 is obtained for the cloudless case.

However, it is dangerous to generalize that Earth's curvature causes event suppression. One sees in the left panel of Fig. 9 that, for high clouds and large cross-section, curvature effects may even *increase* the event rates. This is because more events that would not have been visible above the cloud altitude are now ''lifted'' to visibility, compared to the number of events that would have been visible but are now lifted to invisibility. Curvature does not increase rates in the right panel, which points again to the dangers of generalization.

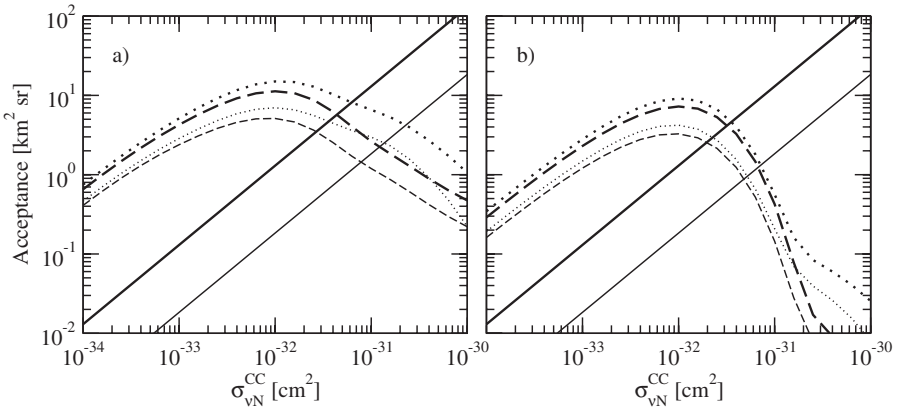

FIG. 9. Dependence of acceptance on cloud altitudes for space-based fluorescence detectors. Fixed values are $l_{\mathrm{min}} = 5$ km, and threshold energies of $E_{\mathrm{th}}^{\mathrm{sh}} = 10^{19}$ eV in the left panel and 5×10^{19} eV in the right panel. All curves representing UAS assume trajectories over water and an initial neutrino energy of 10^{20} eV; curves for HAS are valid for any energy exceeding $E_{\mathrm{th}}^{\mathrm{sh}}$. Solid lines show HAS, while dashed and dotted lines show UAS with and without Earth-curvature effects, respectively. Thick lines are for a cloud layer at 4 km and thin lines for a cloud layer at 12 km.

In Fig. 10, we show dependences of the acceptances on the parameters $l_{\rm min}$ and $d_{\rm min}$ describing the shower triggers, and the parameter $d_{\rm max}$ characterizing shower extinction. In this figure we assume a cloudless sky. Threshold energies are $E_{\rm th}^{\rm sh} = 10^{19}$ eV in the left panel and 5×10^{19} eV in the right panel. Thick curves present HAS acceptances and thin curves present UAS acceptances. All curves representing UAS assume events over water, and an initial neutrino energy of 10^{20} eV; curves for HAS are valid for any energy exceeding $E_{\rm th}^{\rm sh}$. We depict four different sets of shower parameters: $(d_{\rm min}, d_{\rm max}, l_{\rm min}) = (0\ {\rm g/cm^2}, 10^5\ {\rm g/cm^2}, 0\ {\rm km})$ shown in solid curves, $(300\ {\rm g/cm^2}, 1500\ {\rm g/cm^2}, 5\ {\rm km})$ in dashed curves, $(300\ {\rm g/cm^2}, 1500\ {\rm g/cm^2}, 10\ {\rm km})$ in dotted curves, and $(400\ {\rm g/cm^2}, 1200\ {\rm g/cm^2}, 10\ {\rm km})$ in dash-dotted curves. The value $d_{\rm max} = 10^5\ {\rm g/cm^2}$ is to be interpreted as an effectively infinitely long shower persistence, i.e. an illustration of shower development without extinction. The acceptances in the solid curves correspond to the most liberal shower-trigger requirements, with basically all showers declared observable. Those in he dashed, dotted, and dash-dotted curves correspond to a realistic set of choices for the shower-development parameters $d_{\rm min}$, $d_{\rm max}$ and for the shower length $l_{\rm min}$.

One sees that, even in the cloudless case shown here, the dependences on the shower parameters is considerable. The UAS acceptance gets reduced by ~ 2 when $l_{\rm min}$ is increased from 5 to 10 km and the visible column density $(d_{\rm max} - d_{\rm min})$ is reduced from 1200 to 800 g/cm^2. Changes in the HAS acceptance are a bit more dramatic. As the shower triggers are tightened according to our examples, the HAS acceptance falls by a factor ~ 6.

The acceptances in Fig. 10 can also be compared to the thin solid (UAS) and dotted (HAS) curves in panels (b) and (d) of the no-cloud Fig. 7, where $(d_{\rm min}, d_{\rm max}, l_{\rm min}) = (400\ {\rm g/cm^2}, 1200\ {\rm g/cm^2}, 5\ {\rm km})$. As can be seen from this figures, the effect of reducing the constraint on the minimum shower length from 10 to 5 km increases the acceptance in the cloudless sky by roughly a factor of ~ 3 for HAS, and ~ 2 for UAS.

With clouds, the sensitivity to shower-development parameters is more acute. The dotted case corresponds to a good trigger sensitivity (discussed in Sec. IV E) of $(d_{\rm max} - d_{\rm min})/l_{\rm min} = 120\ {\rm g\,cm^{-2}/km}$, and so to a critical cloud altitude of $z_{\rm cloud}^{\rm crit} = 0.56$ km (refer to Fig. 6). The dash-dotted case corresponds to a less good $80\ {\rm g\,cm^{-2}/km}$ sensitivity, and a less pleasing (for ground-based detectors) critical cloud-altitude $z_{\rm cloud}^{\rm crit} = 3.8$ km. Thus one expects the dash-dotted case to be quite sensitive to cloud layers, and the other three cases to be relatively insensitive to cloud layers.

VII. DISCUSSION

In this paper we have presented a mostly analytic calculation of the acceptances of space-based and ground-based fluorescence detectors of air-showers at extreme energies. Included in the calculation are the dependences of the acceptances on initial neutrino energy, trigger threshold for the shower energy, composition of Earth (surface rock or ocean water), and several shower parameters (the minimum and maximum column densities for shower visibility, and the tangent length of the shower). Also included in the calculation are suppression of the acceptances by cloud layers of arbitrary altitude, and in the UAS case, by the Earth's curvature. Most importantly, included in the calculations are the dependences on the unknown neutrino cross-section. The dependence is trivial and linear for HAS, but nontrivial and nonlinear for UAS.

The merits of the analytic construction are twofold: it offers an intuitive understanding of each ingredient entering the total calculation; and it allows one to easily recom-

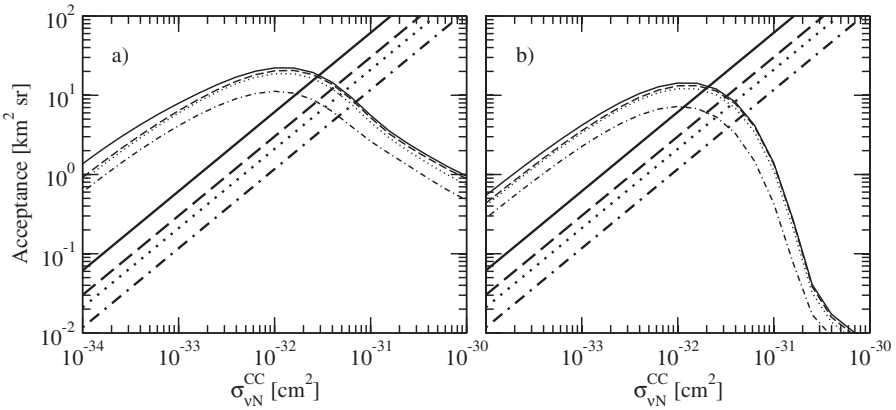

FIG. 10. Dependences on $d_{\rm min}$, $d_{\rm max}$, and $l_{\rm min}$ without clouds of acceptances for space-based fluorescence detectors. Threshold energies are $E_{\rm th}^{\rm sh} = 10^{19}$ eV in the left panel, and 5×10^{19} eV in the right panel. All curves representing UAS assume trajectories over water, and an initial neutrino energy of 10^{20} eV; curves for HAS are valid for any energy exceeding $E_{\rm th}^{\rm sh}$. Thick lines represent HAS, and thin lines UAS. Solid lines correspond to $(d_{\rm min}, d_{\rm max}, l_{\rm min}) = (0\ {\rm g/cm^2}, 10^5\ {\rm g/cm^2}, 0\ {\rm km})$, dashed lines to $(300\ {\rm g/cm^2}, 1500\ {\rm g/cm^2}, 5\ {\rm km})$, dotted lines to $(300\ {\rm g/cm^2}, 1500\ {\rm g/cm^2}, 10\ {\rm km})$, and dash-dotted lines to $(400\ {\rm g/cm^2}, 1200\ {\rm g/cm^2}, 10\ {\rm km})$.

pute when parameters governing the shower or the atmosphere are varied. While a Monte Carlo approach may be simpler to implement, it sacrifices some insight and efficiency.

The differing dependences of HAS and UAS on $\sigma_{\nu N}^{\mathrm{CC}}$ enable two very positive conclusions: (1) the ''no-lose theorem'' is valid, namely, that acceptances are robust for the combined HAS plus UAS signal regardless of the cross-section value; and (2) an inference of the cross-section at 10^{20} eV is possible if HAS and UAS are both measured.

Our formulas are valid for the energy range $\sim 10^{18}$–10^{21} eV. The lower limit is necessary to validate our assumption that the τ decay length is much larger than its radiation length. Below 10^{18} eV, the τ's boost factor is insufficient to provide a τ lifetime in compliance with this assumption. The upper limit arises from the fact that above 10^{21} eV, the weak charged-current losses of the τ's, not included in our calculation, exceed their electromagnetic losses, which we have included. Although the energy range of validity is limited, it covers the range of interest for extreme-energy cosmic neutrino studies.

A. A tale of two media (ocean and land), and two lengths (λ_ν and λ_τ)

One may sensibly ask, ''what difference does it make whether the UAS interaction takes place in water or in rock?'' After all, one has only to look at a different value of L or θ_n to compensate for any change in target density. Nevertheless, we have shown that the UAS rate over ocean is an order of magnitude larger than over land. Let us explore this a bit.

The rate for producing upgoing taus which exit the Earth's surface has its peak near the chord length $L_{\mathrm{peak}} \sim \lambda_\nu + \lambda_\tau$. Increasing the solid angle optimizes the rate. This is accomplished by making L_{peak} as large as possible. Equivalently then, we ask that λ_ν and λ_τ be as large as possible. Explicitly, we seek to maximize

$$L_{\mathrm{peak}} \sim \lambda_\nu + \lambda_\tau = \frac{1}{\rho_{\mathrm{earth}}}\left(\frac{1}{\sigma_{\nu N}^{\mathrm{CC}} N_A} + \frac{1}{\beta_\tau}\right). \tag{100}$$

Apparently, Nature may optimize L_{peak} in one of three ways: either reducing the cross-section, reducing the tau's radiation loss, or reducing the density. Thus, the oceans, less dense than surface rock, will serve to increase the emerging tau rate by the factor $\rho_{\mathrm{sr}}/\rho_{\mathrm{w}} = 2.65$ (for fixed $\sigma_{\nu N}^{\mathrm{CC}}$ and β_τ). For generation of the visible UAS, there is a further enhancement. Trajectories through water exit the Earth nearly horizontally. Horizontally emergent taus have more time and more atmosphere in which to decay and evolve into a visible shower. This further increases the UAS acceptance. There is a third effect: β_τ in water is nearly half of β_τ in rock, leading to a larger λ_τ in Eq. (100). So several effects conspire to enhance the UAS acceptance over water vs over land. In our numerical work presented in Figs. 7 and 8, we found the enhancement to be typically a factor of 10. This enhancement over water is fortunate, in that 70% of the Earth's surface is ocean, and ocean nights are not polluted with manmade lights.

Note that

$$\frac{\lambda_\tau}{\lambda_\nu} = \sigma_{31}\left(\frac{\beta_{19}}{\beta_\tau(E)}\right) \times \begin{cases} 0.06 & \text{for rock} \\ 0.10 & \text{for water.} \end{cases} \tag{101}$$

Furthermore, the energy dependence of $\beta_\tau(E) \propto E^{0.2}$ is mild, changing β_τ by just 1.6 per decade. Thus, we have that $\lambda_\nu > \lambda_\tau$ for $\sigma_{\nu N}^{\mathrm{CC}} \lesssim 10^{-30}$ cm^2, i.e. for the entire range of cross-sections which we consider. So the story of the UAS enhancement over water is really the story of the neutrino's longer MFP in water than in rock, followed by the tau's greater probability to decay and shower following its nearly tangential emergence from water.

For very weak cross-sections, the MFP becomes large compared to the size of the critical chord in the ocean $L_{\mathrm{w\text{-}sr}} = 422\sqrt{z_{\mathrm{w}}/3.5\ \mathrm{km}}$ km (derived in the Appendix), beyond which the neutrino is forced to spend the middle part of its trajectory in rock. This rock component mitigates the difference between UAS over water and over land, and is included in our calculations. The neutrino MFP exceeds the critical chord for $\sigma_{\nu N}^{\mathrm{CC}} < 4 \times 10^{-32}$ cm^2. Far below this cross-section value, the ocean portion of the neutrino's chord is too small to affect the UAS rate. In Fig. 7 one can see that the two UAS acceptances, over water and over land, tend toward each other below $\sigma_{\nu N}^{\mathrm{CC}} \sim 10^{-32}$ cm^2, and to a tenfold enhancement for water above $\sigma_{\nu N}^{\mathrm{CC}} \sim 10^{-32}$ cm^2.

B. Remark on observations over elevated land

We have presented results for events over land and ocean, both taken to have zero, i.e. ''sea level,'' elevation. However, much of the Earth's land surface is at higher elevation (fortunately, for land animals). Furthermore, some ground-based observatories are sited at high elevations to reduce various backgrounds. The Auger observatory in Argentina, for example, is at 1400 m, above $\sim$15% of the atmosphere. The HiRes siting in Utah is at a similar elevation. For HAS viewed from these sites (in cloudless skies), the acceptance is the same as that for space-based viewing with a cloud layer at 1.4 km. For UAS viewed from elevated sites, one cannot proceed by simple analogy.

However, inclusion of elevation into our formalism, for ground-based or space-based, HAS or UAS, with clouds and without, is simple. One merely replaces the sea-level atmospheric density, $\rho(0)$, with the ground-level density. For an elevation of z_{elev}, the replacement value is $e^{-z_{\mathrm{elev}}/h}\rho(0)$. This leads to the further replacement $d_{\mathrm{vert}} \rightarrow e^{-z_{\mathrm{elev}}/h} d_{\mathrm{vert}}$. With these substitutions, all previous formulas may be used, with altitudes of clouds and other ''z-parameters'' now understood to be with respect to ground level, not sea level. Strictly speaking, z_{thin} should be replaced by $z_{\mathrm{thin}} - z_{\mathrm{elev}}$. This would allow accurate

comparisons of acceptances from elevation with those from sea-level. In practice, keeping or not keeping the additional kilometer or so of thin atmosphere makes little difference. For comparing ground-based and space-based detectors at a common elevation, the difference is irrelevant.

In summary, ground elevation reduces the amount of atmospheric volume available, sometimes substantially. This in turn reduces the target mass for HAS, the decay volume for UAS, and the grammage available for shower development. Consequently, elevation disadvantages observations over land, compared to space-based observations over the zero-elevation ocean. The disparity between the two becomes more acute in the presence of clouds.

C. Comparisons with prior work

Among the aims of this paper is the detailed extension of the idea introduced in Ref. [21], that $\sigma_{\nu N}^{\mathrm{CC}}$ at 10^{20} eV can be inferred from a measurement of the UAS/HAS ratio. So let us first compare our calculation with the more qualitative one in Ref. [21], where several energy dependences were purposely frozen, for simplicity. The tau energy loss was set constant $\beta_\tau(E) = \beta_{19}$ (i.e., $\alpha = 0$), and the energy for the produced tau lepton was assumed to be that of the incoming neutrino (i.e., $\langle y \rangle = 0$). The decay length for the taus exiting the Earth was fixed to a single value, ignoring the dependence on the tau's initial energy, production point in the Earth, and zenith angle. Furthermore, all taus were considered to decay within an atmospheric height of 10 km. These approximations do not affect the main conclusions of [21], but do impact the results quantitatively. For example, they lead to unphysical behavior in the UAS rate for high values of the cross-section; for very large $\sigma_{\nu N}^{\mathrm{CC}}$ the incident neutrino must interact with the Earth's surface with probability one, and the UAS acceptance should asymptote to a $\sigma_{\nu N}^{\mathrm{CC}}$-independent constant determined solely by tau physics. Also, the case where the trajectory's chord length in the Earth is smaller than the distance for which the tau lepton energy is reduced to the threshold value E_{th}^{τ}, is incorrectly calculated. The impact of this is small, for it only affects very Earth-skimming neutrinos ($\theta_{\mathrm{hor}} < 0.1^\circ$). Finally, Ref. [21] only considered neutrinos traveling through rock, not water, and did not include suppression effects from realistic shower formation, clouds, or curvature of the Earth. Our work considerably improves upon the original work of Ref. [21].

The prior work in Refs. [31,33,42] (and related work in Ref. [43]) is semianalytic, like our own. A main difference between them and us is the manner in which the tau energy loss is parametrized. The parameter β_τ is taken to be constant in Ref. [42] (where $\langle y \rangle = 0$ is also assumed), to depend linearly on the tau energy in Ref. [33], and assigned a logarithmic dependence on the energy in Ref. [31]. Also, Refs. [33,42] assume some maximum tau decay distance, and do not implement any constraints from the subsequent shower formation. Furthermore, they do not consider events over water, or the presence of clouds. Reference [31] computes the flux of tau leptons exiting the Earth, but does not consider the important process of tau decay and shower formation. On the other hand, [31] does include the possibility of the tau decaying inside the Earth. However, as we mentioned earlier in our paper, including tau decay within the Earth reduces the UAS acceptance by less than a few per cent for the energies of interest here. Also in Ref. [31], a Monte Carlo calculation is performed and shown to agree with the semianalytical approach to very good accuracy. Where comparisons are possible, our results agree qualitatively with [31]. Let us note that Ref. [44] offers an improved and more detailed evaluation of the effective acceptance for fluorescence detection at the Pierre Auger Observatory (PAO). Taken into account is the real elevation profile of the surrounding mountains. They find a significant increase in the event rate due to the nearby mountains, compared to the semianalytical, mountainless calculations of Refs. [33,42] and us. Unfortunately, even with the enhancement, the predicted PAO event rates are $\lesssim 0.5$ events/yr for neutrino fluxes motivated by the GZK process and topological defect decay models. This small rate points again to one of the major benefits of space-based detectors: the much larger FOV.

In Ref. [45], a detailed semianalytical computation of UAS and HAS was performed. This work considered a larger range of energies than we do. Hence, it was necessary for Ref. [45] to include the possibility of tau decay inside the Earth. This work assumed β_τ to be constant, but otherwise the energy loss of the produced tau was calculated accurately. In addition, constraints on the shower formation were included in a semianalytical approach, in order to calculate event rates for an air-shower array. The main differences between this work and our calculation is that we consider a water layer as well as rock, and we include the possibility of clouds.

Detailed Monte Carlo simulations of acceptances are presented in Refs. [30,46]. Neutrino scattering inelasticities and tau energy losses are accurately included. We have checked that we get very good agreement with the results of these papers. Reference [30] is specific to the ground-based PAO detector. It includes realistic shower formation and detector response, but it does not consider clouds. It also considers only neutrino and tau propagation in rock. While rock is the dominant material in the vicinity of Auger, there are trajectories reaching Auger from the West which will travel in the Pacific Ocean. Reference [46], undertaken mainly with EUSO in mind, does study acceptances over both water and land.

In Ref. [47], the analytic approach is different, and more optimistic rates are obtained. However, there are several questionable approximations. How the energy threshold

constraint is implemented is obscure. The treatment of the Earth's atmosphere is too simplistic. Although the calculation is meant to be valid for an arbitrary Earth density profile, the derived expression for the event number is only valid for a constant Earth density. Our acceptances for UAS events do not support the optimistic UAS rates of Ref. [47]. We do however support the results found by the more detailed analyses, e.g. that in Ref. [46].

In summary, the main advances we present in our study are the inclusion of a new analytic and accurate power-law parametrization for the tau energy-loss prestaging UAS events, the analytical implementation of shower constraints, cloud boundaries, and Earth curvature, and the consideration of UAS events over the ocean as well as over land. We note that the tau energy-loss parametrization we implement in the present study was already used in Ref. [30] for the case of taus propagating in rock. Here we present also the parametrization when taus cross a water layer.

D. Odds and ends

In this subsection we offer remarks on issues possibly relevant to this paper.

1. Incident neutrino flavor ratios

One of the main points of this paper is to hone the argument that the CC neutrino cross-section can be inferred from a comparison of UAS and HAS rates. The ratio of these rates is the product of a flux ratio times acceptance ratio. We have focused on the electron-neutrino as the primary particle for HAS initiation, and the tau neutrino as the primary particle for UAS initiation, for the good reasons given in the text. The relevant flux ratio, therefore, is the ratio of the ν_e flux to the ν_τ flux.

We have calculated acceptances. From these, one may simply form the acceptance ratio. What is not known at present is the relevant ν_e to ν_τ flux ratio at $\sim 10^{20}$ eV. A general theorem for neutrino flavor mixing states that if the atmospheric mixing angle is nearly maximal (it is), and if the short-baseline angle θ_{13} is nearly zero (it is), then ν_μ and ν_τ equilibrate over cosmic distances. A corollary to the theorem then is that, if cosmic neutrinos originate from the complete pion decay chain, $\pi \to \mu + \nu_\mu \to e + \nu_e + 2\nu_\mu$, then after equilibration the neutrinos will arrive at Earth with the democratic flavor ratio of 1:1:1. However, dynamics at the source, or new physics en route from the source, could alter this favorable ratio. *Caveat emptor.*

2. Ratio of neutral- and charged-current cross-sections

It is an implicit assumption in this work that the ratio of the neutral to charged-current cross-section is small, ~ 0.44 according to the standard model of particle physics. However, it is possible that above 10^{15} eV and below 10^{20} eV a threshold is passed at which the NC interaction becomes strong and the CC interaction does not. Such would be the case, for example, in models of low-scale gravity unification.

Crossing such a hypothetical threshold would change the physics in this paper dramatically. First of all, even though the NC interaction typically puts ~ 5 times less energy into the shower than does the ν_e CC interaction, with a much larger NC cross-section, even at fixed $E^{\rm sh}$ the NC events would dominate the ν_e CC events. Secondly, UAS acceptances would be reduced because the energy losses of neutrinos passing through the Earth would be larger.

3. Weakly interacting non-neutrino primaries

The range of cross-sections we consider in this work spans the cross-sections of weakly interacting massive particles (WIMP), a popular candidate for dark matter. We believe, therefore, that our figures may be useful in assessing the qualitative features of acceptances for WIMP detection. However, we caution that there are substantial differences between WIMP initiation of showers and neutrino initiation. The WIMP carries considerable inertial mass, and so transfers less energy to its shower. Also, the UAS generated by a WIMP flux would likely not proceed through the tau production and decay chain.

VIII. CONCLUSIONS

We have presented analytic formulas for the acceptances of fluorescence detectors, both space-based and ground-based, for neutrino-initiated events, as a function of the unknown extreme-energy neutrino cross-section. For the downgoing HAS events, the dependence of acceptance on cross-section is linear, but for upcoming UAS events the acceptance is quite complicated. It turns out to be somewhat flat and relatively large, which validates the ''cannot lose'' theorem which says that, if the HAS rate is suppressed by a small $\sigma^{\rm CC}_{\nu N}$, then the UAS rate compensates to establish a robust signal.

We have studied the dependence of acceptances on the incident neutrino energy, the trigger-energy $E^{\rm sh}_{\rm th}$ for the shower, shower-development parameters $d_{\rm min}$ and $d_{\rm max}$, and observable (tangent) shower length $l_{\rm min}$; and on the ''environmental'' conditions of cloud layers for HAS and UAS, and events over ocean versus over land for UAS. UAS showers typically originate at a considerable distance ($c\tau_\tau = 4900(E_\tau/10^{20}$ eV) km) from the point on the Earth where the parent tau emerged. Therefore, due to the Earth's curvature, they originate at higher altitudes with thinner air. Thus, it is necessary to include the Earth's curvature in the calculation of UAS acceptances. We have done so. We find that inclusion of the Earth's curvature reduces the UAS acceptance by a factor of a few when $\sigma^{\rm CC}_{\nu N} \gtrsim 0.5 \times 10^{-31}$ cm^2. The meaning of ''a few'' depends on the various parameters entering the calculation.

Clearly, lower shower-trigger energies are better. This is especially true when clouds are present. We have quanti-

fied the sensitivity to $E_{\rm th}^{\rm sh}$ by comparing two realistic values, 10^{19} and 5×10^{19} eV in the face of incident neutrino energies of 10^{20} and 10^{21} eV.

Cloud layers may severely suppress acceptances. For UAS acceptances, there is a strong dependence on the combination of shower-trigger parameters $(d_{\rm max} - d_{\rm min})/l_{\rm min}$, especially with clouds present. Maximizing this combination to a value of $d_{\rm vert}/h = \rho(0) = 129\,{\rm g\,cm^{-2}/km}$ or greater significantly minimizes the suppression from clouds. For $(d_{\rm max} - d_{\rm min})/l_{\rm min} \lesssim \rho(0)$, there is a critical altitude $z_{\rm cloud}^{\rm crit}({\rm UAS}) \equiv -h \ln[((d_{\rm max} - d_{\rm min})/l_{\rm min}) \times (h/d_{\rm vert})]$ below which a cloud layer would totally obscure the acceptance of a ground-based UAS detector, but leave the acceptance of a space-based UAS detector unaltered. Clouds above the critical altitude would partially obscure UAS events, and therefore suppress the acceptances, of both space-based and ground-based detectors.

Concerning UAS events over water versus over land, we find that acceptances over water are larger, typically by an order of magnitude. We have traced this enhancement over water to the increased path length in water of both neutrinos and taus, and to the increased path length in air for tau decay and increased column density in air for shower development, when a tau emerges with small horizontal angle from the relatively shallow ocean. We also noted the smaller enhancement from the fact that the atmospheric grammage over water integrates from sea level, whereas the grammage over land is often 15% less. It is difficult to imagine a ground-based detector over the ocean, so the ''water advantage'' clearly belongs to the orbiting space-based detectors. Perhaps a ground-based detector could be positioned near an ocean to realize the ''water advantage'' for much of its solid angle.

In the spirit with which we began this study, we are led to two bottom-line conclusions:

(i) Inference of the neutrino cross-section at and above 10^{20} eV from the ratio of UAS and HAS events appears feasible, assuming that a neutrino flux exists at these energies.

(ii) Space-based detectors enjoy advantages over ground-based detectors for enhancing the event rate. The advantages are a much higher UAS rate over water compared to land, and the obvious advantage that space-based FOV's greatly exceed ground-based FOV's.

Our hope is that space-based fluorescence detection becomes a reality, so that the advantages of point (ii) can be used to discover/explore the extreme-energy cosmic neutrino flux. According to point (i), part of the discovery/exploration can be the inference of the neutrino cross-section at $E_\nu \sim 10^{20}$ eV.

ACKNOWLEDGMENTS

Encouragement from J. Adams, S. Bottai, O. Catalano, D. Cline, D. Fargion, P. Lipari, A. Santangelo, L. Scarsi, Y. Takahashi, and the EUSO community is acknowledged. Figure 1 was contributed by Liguo Song. S. P. R. and T. J. W. are supported by NASA Grant No. ATP02-0000-0151 for EUSO studies, S. P. R. by the Spanish Grant No. FPA2002-00612 of the MCT, and T. J. W. by the U.S. Department of Energy Grant No. DE-FG05-85ER40226.

APPENDIX: DENSITY INTEGRATIONS IN THE EARTH

Two column densities in the Earth are of relevance for UAS probabilities. The first is the path integral of $\rho_{\rm earth}$ for the incident neutrino from entrance to interaction in the Earth. This column density controls the neutrino absorption probability, and therefore, the neutrino survival probability to the point of interaction $w_{\rm int}$. The column density $d_\nu(\theta_n)$ is stated in Eq. (6) as

$$d_\nu(\theta_n) = \int_{w_{\rm int}}^{L} dw \rho_{\rm earth}(w). \tag{A1}$$

For constant density, which applies only for Earth-skimming neutrinos entirely in surface rock ($\rho_{\rm earth} = \rho_{\rm sr} = 2.65\ {\rm g/cm^3}$) or entirely in ocean water ($\rho_{\rm earth} = \rho_{\rm w} = 1.0\ {\rm g/cm^3}$), the result is simply $d_\nu(\theta_n) = (L - w_{\rm int})\rho_{\rm earth}$. This constant density result holds in ocean for angles relative to the horizon smaller than 1.90°, and it holds in rock for angles relative to the horizon smaller than 22.17°, as we show below.

The second relevant column density in the Earth is that of the emerging tau in the UAS event sequence. This column density $d_\tau(\theta_n)$ is the path integral of $\rho_{\rm earth}$ from the interaction point in the earth to the earth's surface,

$$d_\tau(\theta_n) = \int_{0}^{w_{\rm int}} dw \rho_{\rm earth}(w). \tag{A2}$$

For constant density, which applies for taus emerging from rock, or for taus emerging from water with horizon angle less than 1.90°, the result is simply $d_\tau(\theta_n) = w_{\rm int}\rho_{\rm earth}$. This column density, when suitably weighted with the tau energy-attenuation factor $\beta_\tau(E)$, controls the tau energy-loss probability, and therefore, the probably for the tau energy and lifetime at emergence from the Earth as given in Eqs. (8) and (12).

For our purposes, concentric shells of constant density provide a sufficiently accurate approximation to the Earth's profile, and allow for an analytic evaluation of the path integrals. We take a simple model of this kind for the Earth density:

$$\rho_{\rm earth}(r) = \begin{cases} \rho_{\rm w} = 1.0\,{\rm g/cm^3} & \text{for } r_{\rm sr} \equiv R_\oplus - z_{\rm w} < r \le R_\oplus, \\ \rho_{\rm sr} = 2.65\,{\rm g/cm^3} & \text{for } r_{\rm m} < r \le r_{\rm sr}, \\ \rho_{\rm m} = 4.0\,{\rm g/cm^3} & \text{for } r_{\rm c} < r \le r_{\rm m}, \\ \rho_{\rm c} = 12.0\,{\rm g/cm^3} & \text{for } 0 < r \le r_{\rm c}, \end{cases} \tag{A3}$$

with the radii of the boundaries listed in Table IV. For UAS

TABLE IV. Critical chord lengths and nadir and horizon angles for the indicated Earth boundaries.

Boundary	Radius	Critical L	Critical θ_n	Critical $\theta_{\rm hor}$
Earth/atmosphere	$R_\oplus = 6371$ km	0 km	90°	0°
Water/surface-rock	$r_{\rm sr} = R_\oplus - z_{\rm w}$, $z_{\rm w} = 3.5$ km	$L_{\text{w-sr}} \equiv 422(\frac{z_{\rm w}}{3.5\ {\rm km}})^{1/2}$ km	88.10°	$1.90°(\frac{z_{\rm w}}{3.5\ {\rm km}})^{1/2}$
Surface-rock/mantle	$r_{\rm m} = 5900$ km	$L_{\text{sr-m}} \equiv 4808$ km	67.8°	22.2°
Mantle/core	$r_{\rm c} = 3486$ km	$L_{\text{m-c}} \equiv 10\,700$ km	33.2°	56.8°

events over land, we replace the outermost $z_{\rm w} = 3.5$ km of water with surface rock. Thus, there are in this Earth model four (three) concentric density zones for UAS events over water (land).

The chord length L, nadir angle θ_n, and horizon angle $\theta_{\rm hor}$ are related to the sagitta s (the depth measured perpendicular to the Earth's surface) by the formulas

$$L(s) = 2\sqrt{2R_\oplus s - s^2}, \tag{A4}$$

$$\cos\theta_n(s) = \sin\theta_{\rm hor}(s) = \sqrt{2\frac{s}{R_\oplus} - \left(\frac{s}{R_\oplus}\right)^2}, \tag{A5}$$

$$\sin\theta_n(s) = \cos\theta_{\rm hor}(s) = 1 - \frac{s}{R_\oplus}; \tag{A6}$$

and to the boundary radius $r_{\rm B}$ by

$$L(r_{\rm B}) = 2\sqrt{R_\oplus^2 - r_{\rm B}^2}, \tag{A7}$$

$$\cos\theta_n(r_{\rm B}) = \sin\theta_{\rm hor}(r_{\rm B}) = \sqrt{1 - \left(\frac{r_{\rm B}}{R_\oplus}\right)^2}, \tag{A8}$$

$$\sin\theta_n(r_{\rm B}) = \cos\theta_{\rm hor}(r_{\rm B}) = \frac{r_{\rm B}}{R_\oplus}. \tag{A9}$$

In Table IV we collect the critical values for L and θ_n at the various boundary layers.

A further useful formula is the path length $w(r_{\rm B}; L)$ from the Earth's surface to the boundary of radius $r_{\rm B}$, for fixed L or θ_n:

$$w(r_{\rm B}; L \text{ or } \theta_n) = \frac{L}{2} - \sqrt{\left(\frac{L}{2}\right)^2 + r_{\rm B}^2 - R_\oplus^2}, \tag{A10}$$

$$= R_\oplus\cos\theta_n - \sqrt{r_{\rm B}^2 - R_\oplus^2\sin^2\theta_n}. \tag{A11}$$

Consider the calculation of the total column density along a chord, $d_{\rm tot}(L)$. Using the path lengths defined in Eq. (A10), the result is

$$d_{\rm tot} = \begin{cases} L\rho_{\rm w}, & \text{for } 0 \le L \le L_{\text{w-sr}} \\ 2\left\{w(r_{\rm sr}; L)\rho_{\rm w} + \left[\frac{L}{2} - w(r_{\rm sr}; L)\right]\rho_{\rm sr}\right\}, & \text{for } L_{\text{w-sr}} < L \le L_{\text{sr-m}} \\ 2\left\{w(r_{\rm sr}; L)\rho_{\rm w} + [w(r_{\rm m}; L) - w(r_{\rm sr}; L)]\rho_{\rm sr} + \left[\frac{L}{2} - w(r_{\rm m}; L)\right]\rho_{\rm m}\right\}, & \text{for } L_{\text{sr-m}} < L \le L_{\text{m-c}} \\ 2\left\{w(r_{\rm sr})\rho_{\rm w} + [w(r_{\rm m}) - w(r_{\rm sr})]\rho_{\rm sr} + [w(r_{\rm c}) - w(r_{\rm m})]\rho_{\rm m} + \left[\frac{L}{2} - w(r_{\rm c})\right]\rho_{\rm c}\right\}, & \text{for } L_{\text{m-c}} < L \le 2R_\oplus \end{cases} \tag{A12}$$

where, for compactness, we have suppressed the L-dependence of the w-function in the final line. For events over land, $\rho_{\rm w}$ must be replaced in Eq. (A12) with $\rho_{\rm sr}$.

Next we consider the calculation of $d_\tau(L)$. The tau radiation length is very short on the scale of $r_{\rm m}$, and so the tau path is confined to just surface rock and ocean. Over land, then, we have simply $d_\tau(\text{land}) = w_{\rm int}\rho_{\rm sr}$. Over water, the calculation has two contributions in general, from water and from surface rock. For $L < L_{\text{w-sr}}$, the tau encounters just water, and so $d_\tau(\text{ocean}; L < L_{\text{w-sr}}) = w_{\rm int}\rho_{\rm w}$. For $L > L_{\text{w-sr}}$, the tau encounters rock and then water. However, the tau never encounters first water and then rock and then water again, for this requires a tau trajectory exceeding $1/2$ of the critical path length $L_{\text{w-sr}}$, which is $211(\frac{z_{\rm w}}{3.5\ {\rm km}})^{1/2}$ km, far exceeding the tau radiation length. We summarize these results, again making use of Eq. (A10):

$$d_\tau = \begin{cases} w_{\rm int}\rho_{\rm sr}, & \text{over land,} \quad \text{for all } w_{\rm int} \\ w_{\rm int}\rho_{\rm w}, & \text{over oceans,} \quad \text{for } w_{\rm int} < w(r_{\rm sr}; L) \\ w(r_{\rm sr}; L)\rho_{\rm w} + [w_{\rm int} - w(r_{\rm sr}; L)]\rho_{\rm sr}, & \text{over oceans,} \quad \text{for } w_{\rm int} > w(r_{\rm sr}; L). \end{cases} \tag{A13}$$

To obtain d_ν, we may use the simple relation $d_\nu = d_{\rm tot} - d_\tau$. Thus, we are finished with calculating column densities.

The tau opacity defined in Eq. (9) is easily obtained in the constant-density concentric-shells approximation. Weighting the segments in Eq. (A13) with the corresponding values of β_{19}, either $\beta_{19}^{\rm sr} = 1.0 \times 10^{-6}$ cm^2/g or $\beta_{19}^{\rm w} = 0.55 \times 10^{-6}$ cm^2/g, we have

$$\mathcal{I}(w_{\rm int}) = \begin{cases} w_{\rm int}\beta_{19}^{\rm sr}\rho_{\rm sr}, & \text{over land,} \quad \text{for all } w_{\rm int} \\ w_{\rm int}\beta_{19}^{\rm w}\rho_{\rm w}, & \text{over oceans,} \quad \text{for } w_{\rm int} < w(r_{\rm sr}; L) \\ w(r_{\rm sr}; L)\beta_{19}^{\rm w}\rho_{\rm w} + [w_{\rm int} - w(r_{\rm sr}; L)]\beta_{19}^{\rm sr}\rho_{\rm sr}, & \text{over oceans,} \quad \text{for } w_{\rm int} > w(r_{\rm sr}; L). \end{cases} \tag{A14}$$

We also need an explicit formula for $w_{\rm th}(L)$, defined implicitly in Eqs. (9) and (10). For notational brevity, let us recall the notation in Eq. (10):

$$\mathcal{I}(w_{\rm th}) \equiv \frac{1}{\alpha}\left[\left(\frac{10^{19}\ {\rm eV}}{E_{\rm th}^\tau}\right)^\alpha - \left(\frac{10^{19}\ {\rm eV}}{0.8E_\nu}\right)^\alpha\right]. \tag{A15}$$

Then, a calculation similar to the ones above leads to

$$w_{\rm th}(L) = \begin{cases} \frac{1}{\beta_{19}^{\rm sr}\rho_{\rm sr}}\mathcal{I}(w_{\rm th}), & \text{over land,} \quad \text{for all } L, \\ \frac{1}{\beta_{19}^{\rm w}\rho_{\rm w}}\mathcal{I}(w_{\rm th}), & \text{over oceans,} \quad \text{for } L \le L_{\text{w-sr}} \text{ or } \mathcal{I}(w_{\rm th}) < \beta_{19}^{\rm w}\rho_{\rm w}w(r_{\rm sr}; L), \\ w(r_{\rm sr}; L)\left(1 - \frac{\beta_{19}^{\rm w}\rho_{\rm w}}{\beta_{19}^{\rm sr}\rho_{\rm sr}}\right) + \frac{1}{\beta_{19}^{\rm sr}\rho_{\rm sr}}\mathcal{I}(w_{\rm th}), & \text{over oceans,} \quad \text{for } L > L_{\text{w-sr}} \text{ and } \mathcal{I}(w_{\rm th}) > \beta_{19}^{\rm w}\rho_{\rm w}w(r_{\rm sr}; L). \end{cases} \tag{A16}$$

Finally we note that, in all the above formulas for events over oceans, the correct result over land may be found by simply setting $\rho_{\rm w}$ equal to $\rho_{\rm sr}$ and $\beta_{19}^{\rm w}$ equal to $\beta_{19}^{\rm sr}$.

[1] K. Greisen, Phys. Rev. Lett. **16**, 748 (1966).

[2] G. T. Zatsepin and V. A. Kuzmin, Pis'ma Zh. Eksp. Teor. Fiz. **4**, 114 (1966) [JETP Lett. **4**, 78 (1966)].

[3] A. Letessier-Selvon, AIP Conf. Proc. **566**, 157 (2001).

[4] T. Abu-Zayyad *et al.* (High Resolution Fly's Eye Collaboration), Astropart. Phys. **23**, 157 (2005).

[5] D. J. Bird *et al.*, Astrophys. J. **441**, 144 (1995).

[6] J. F. Beacom, N. F. Bell, D. Hooper, S. Pakvasa, and T. J. Weiler, Phys. Rev. D **68**, 093005 (2003); **72**, 019901(E) (2005).

[7] For some recent discussions of this assumption, see L. A. Anchordoqui, H. Goldberg, F. Halzen, and T. J. Weiler, Phys. Lett. B **621**, 18 (2005); J. P. Rachen and P. Meszaros, Phys. Rev. D **58**, 123005 (1998); T. Kashti and E. Waxman, Phys. Rev. Lett. **95**, 181101 (2005).

[8] J. F. Beacom, N. F. Bell, D. Hooper, S. Pakvasa, and T. J. Weiler, Phys. Rev. Lett. **90**, 181301 (2003).

[9] J. F. Beacom, N. F. Bell, D. Hooper, J. G. Learned, S. Pakvasa, and T. J. Weiler, Phys. Rev. Lett. **92**, 011101 (2004).

[10] The use of fluorescence profiles to infer ultrahigh cosmic ray energies has recently been validated with electron bunches at SLAC: J. Belz *et al.*, Astropart. Phys. **25**, 57 (2006).

[11] R. Gandhi, C. Quigg, M. H. Reno, and I. Sarcevic, Phys. Rev. D **58**, 093009 (1998).

[12] A. Z. Gazizov and S. I. Yanush, Phys. Rev. D **65**, 093003 (2002); M. H. Reno, I. Sarcevic, G. Sterman, M. Stratmann, and W. Vogelsang, in *Proceedings of the APS/DPF/DPB Summer Study on the Future of Particle Physics, Snowmass, 2001*, edited by N. Graf, eConf C010630, P508 (2001); R. Basu, D. Choudhury, and S. Majhi, J. High Energy Phys. 10 (2002) 012; J. Jalilian-Marian, Phys. Rev. D **68**, 054005 (2003); **70**, 079903(E) (2004); R. Fiore, L. L. Jenkovszky, A. Kotikov, F. Paccanoni, A. Papa, and E. Predazzi, Phys. Rev. D **68**, 093010 (2003); M. V. T. Machado, Phys. Rev. D **71**, 114009 (2005).

[13] L. V. Gribov, E. M. Levin, and M. G. Ryskin, Phys. Rep. **100**, 1 (1983); A. H. Mueller and J. W. Qiu, Nucl. Phys. **B268**, 427 (1986).

[14] L. Anchordoqui and H. Goldberg, Phys. Rev. D **65**, 047502 (2002); L. A. Anchordoqui, J. L. Feng, H. Goldberg, and A. D. Shapere, Phys. Rev. D **65**, 124027 (2002).

[15] E. J. Ahn, M. Cavaglia, and A. V. Olinto, Phys. Lett. B **551**, 1 (2003); P. Jain, S. Kar, and S. Panda, Int. J. Mod. Phys. D **12**, 1593 (2003); L. A. Anchordoqui, J. L. Feng, and H. Goldberg, Phys. Lett. B **535**, 302 (2002).

[16] H. Aoyama and H. Goldberg, Phys. Lett. B **188**, 506 (1987); A. Ringwald, Nucl. Phys. **B330**, 1 (1990); O. Espinosa, Nucl. Phys. **B343**, 310 (1990); L. D. McLerran, A. I. Vainshtein, and M. B. Voloshin, Phys. Rev. D **42**, 171 (1990); P. B. Arnold and M. P. Mattis, Phys. Rev. D **42**, 1738 (1990); V. V. Khoze and A. Ringwald, Phys. Lett. B **259**, 106 (1991); S. Y. Khlebnikov, V. A. Rubakov, and P. G. Tinyakov, Nucl. Phys. **B350**, 441 (1991); A. Ringwald, Phys. Lett. B

555, 227 (2003); F. Bezrukov, D. Levkov, C. Rebbi, V. A. Rubakov, and P. Tinyakov, Phys. Lett. B **574**, 75 (2003); A. Ringwald, J. High Energy Phys. 10 (2003) 008; Z. Fodor, S. D. Katz, A. Ringwald, and H. Tu, Phys. Lett. B **561**, 191 (2003); T. Han and D. Hooper, Phys. Lett. B **582**, 21 (2004).

[17] G. Domokos and S. Nussinov, Phys. Lett. B **187**, 372 (1987); G. Domokos and S. Kovesi-Domokos, Phys. Rev. D **38**, 2833 (1988); J. Bordes, H. M. Chan, J. Faridani, J. Pfaudler, and S. T. Tsou, hep-ph/9705463; Astropart. Phys. **8**, 135 (1998).

[18] G. Domokos and S. Kovesi-Domokos, Phys. Rev. Lett. **82**, 1366 (1999); G. Domokos, S. Kovesi-Domokos, W. S. Burgett, and J. Wrinkle, J. High Energy Phys. 07 (2001) 017.

[19] S. Nussinov and R. Shrock, Phys. Rev. D **59**, 105002 (1999); P. Jain, D. W. McKay, S. Panda, and J. P. Ralston, Phys. Lett. B **484**, 267 (2000); M. Kachelriess and M. Plumacher, Phys. Rev. D **62**, 103006 (2000); L. Anchordoqui, H. Goldberg, T. McCauley, T. Paul, S. Reucroft, and J. Swain, Phys. Rev. D **63**, 124009 (2001); A. V. Kisselev and V. A. Petrov, Eur. Phys. J. C **36**, 103 (2004).

[20] H. Goldberg and T. J. Weiler, Phys. Rev. D **59**, 113005 (1999).

[21] A. Kusenko and T. J. Weiler, Phys. Rev. Lett. **88**, 161101 (2002).

[22] D. Hooper, Phys. Rev. D **65**, 097303 (2002); L. A. Anchordoqui, Z. Fodor, S. D. Katz, A. Ringwald, and H. Tu, J. Cosmol. Astropart. Phys. 06 (2005) 013; L. Anchordoqui and F. Halzen, hep-ph/0510389 [Ann. Phys. (to be published)].

[23] L. A. Anchordoqui, J. L. Feng, H. Goldberg, and A. D. Shapere, Phys. Rev. D **66**, 103002 (2002); L. Anchordoqui, T. Han, D. Hooper, and S. Sarkar, Astropart. Phys. **25**, 14 (2006); and the last reference in [22].

[24] I. Abt *et al.* (H1 Collaboration), Nucl. Phys. **B407**, 515 (1993); T. Ahmed *et al.* (H1 Collaboration), Nucl. Phys. **B439**, 471 (1995); S. Aid *et al.* (H1 Collaboration), Phys. Lett. B **354**, 494 (1995); M. Derrick *et al.* (ZEUS Collaboration), Phys. Lett. B **316**, 412 (1993); M. Derrick *et al.* (ZEUS Collaboration), Z. Phys. C **65**, 379 (1995); M. Derrick *et al.* (ZEUS Collaboration), Phys. Lett. B **345**, 576 (1995); C. Adloff *et al.* (H1 Collaboration), Eur. Phys. J. C **21**, 33 (2001). The neutrino cross-section inferred from HERA data is discussed in D. A. Dicus, S. Kretzer, W. W. Repko, and C. Schmidt, Phys. Lett. B **514**, 103 (2001).

[25] C. Barbot, M. Drees, F. Halzen, and D. Hooper, Phys. Lett. B **563**, 132 (2003).

[26] P. Lipari and T. Stanev, Phys. Rev. D **44**, 3543 (1991); P. Antonioli, C. Ghetti, E. V. Korolkova, V. A. Kudryavtsev, and G. Sartorelli, Astropart. Phys. **7**, 357 (1997); I. A. Sokalski, E. V. Bugaev, and S. I. Klimushin, Phys. Rev. D **64**, 074015 (2001).

[27] S. I. Dutta, M. H. Reno, I. Sarcevic, and D. Seckel, Phys. Rev. D **63**, 094020 (2001).

[28] E. V. Bugaev and Y. V. Shlepin, Phys. Rev. D **67**, 034027 (2003).

[29] K. S. Kuzmin, K. S. Lokhtin, and S. I. Sinegovsky, Int. J. Mod. Phys. A **20**, 6956 (2005).

[30] X. Bertou, P. Billoir, O. Deligny, C. Lachaud, and A. Letessier-Selvon, Astropart. Phys. **17**, 183 (2002).

[31] S. I. Dutta, Y. Huang, and M. H. Reno, Phys. Rev. D **72**, 013005 (2005).

[32] R. Gandhi, C. Quigg, M. H. Reno, and I. Sarcevic, Astropart. Phys. **5**, 81 (1996).

[33] C. Aramo, A. Insolia, A. Leonardi, G. Miele, L. Perrone, O. Pisanti, and D. V. Semikoz, Astropart. Phys. **23**, 65 (2005).

[34] M. Aoki, K. Hagiwara, K. Mawatari, and H. Yokoya, Nucl. Phys. **B727**, 163 (2005).

[35] ESA and EUSO Team, 2000, ESA/MSM-GU/2000.462/ AP/RDA, http://www.euso-mission.org; P. Gorodetzky (The EUSO Collaboration), Nucl. Phys. B, Proc. Suppl. **151**, 401 (2006); G. D'Ali Staiti (EUSO Collaboration), Nucl. Phys. B, Proc. Suppl. **136**, 415 (2004).

[36] T. Abu-Zayyad, C. C. H. Jui, and E. C. Loh, Astropart. Phys. **21**, 163 (2004).

[37] F. W. Stecker, J. F. Krizmanic, L. M. Barbier, E. Loh, J. W. Mitchell, P. Sokolsky, and R. E. Streitmatter, Nucl. Phys. Proc. Suppl. **136B**, 433 (2004).

[38] O. E. Kalashev, V. A. Kuzmin, D. V. Semikoz, and G. Sigl, Phys. Rev. D **66**, 063004 (2002); D. V. Semikoz and G. Sigl, J. Cosmol. Astropart. Phys. 04 (2004) 003.

[39] E. Waxman and J. N. Bahcall, Phys. Rev. D **59**, 023002 (1999); **64**, 023002 (2001). A modification of the WB flux, accommodating the apparent lower-energy crossover from galactic to extragalactic cosmic rays, is given in M. Ahlers, L. A. Anchordoqui, H. Goldberg, F. Halzen, A. Ringwald, and T. J. Weiler, Phys. Rev. D **72**, 023001 (2005).

[40] G. T. Zatsepin, Phys. Lett. **28B**, 423 (1969); R. Engel, D. Seckel, and T. Stanev, Phys. Rev. D **64**, 093010 (2001).

[41] The enhancement of the UAS rate over the ocean relative to over land has been noted in D. Fargion, P. G. De Sanctis Lucentini, and M. De Santis, Astrophys. J. **613**, 1285 (2004).

[42] J. L. Feng, P. Fisher, F. Wilczek, and T. M. Yu, Phys. Rev. Lett. **88**, 161102 (2002).

[43] J. J. Tseng, T. W. Yeh, H. Athar, M. A. Huang, F. F. Lee, and G. L. Lin, Phys. Rev. D **68**, 063003 (2003); N. Gupta, Phys. Rev. D **68**, 063006 (2003); J. Jones, I. Mocioiu, M. H. Reno, and I. Sarcevic, Phys. Rev. D **69**, 033004 (2004).

[44] G. Miele, S. Pastor, and O. Pisanti, Phys. Lett. B **634**, 137 (2006).

[45] E. Zas, New J. Phys. **7**, 130 (2005).

[46] S. Bottai and S. Giurgola, Astropart. Phys. **18**, 539 (2003).

[47] D. Fargion, M. Khlopov, R. Konoplich, P. G. De Sanctis Lucentini, M. De Santis, and B. Mele, Recent Res. Dev. Astrophys. **1**, 395 (2003); D. Fargion, P. G. De Sanctis Lucentini, M. De Santis, and M. Grossi, Astrophys. J. **613**, 1285 (2004).